LA-UR-21-26447
Approved for public release; distribution is unlimited.

Title: Predicting thermodynamic and thermophysical properties of molten chloride salts from ab-initio and classical molecular dynamics simulations

Author(s): Andersson, Anders David Ragnar
Jiang, Chao

Intended for: Report

Issued: 2021-08-12 (rev.1)

# Predicting thermodynamic and thermophysical properties of molten chloride salts from ab-initio and classical molecular dynamics simulations

D. Andersson[a] and C. Jiang[b]

[a]Materials Science and Technology Division, Los Alamos National Laboratory P.O. Box 1663, Los Alamos, NM 87545, USA
[b]Computational Mechanics and Materials Department, Idaho National Laboratory, Idaho Falls, ID 83415, USA

# Contents

# 1 Introduction

Molten salt reactors (MSRs) are among the advanced concepts pursued under the generation IV nuclear energy technology umbrella. However, the basic concept is not new and was first developed as part of the effort to power aircrafts with nuclear energy in the 1950's. Later in the 1960's, Oak Ridge National Laboratory (ORNL) built and operated the Molten-Salt Reactor Experiment (MSRE) [1]. This reactor used a fluoride salt with uranium as fuel. Fluorides salts are still highly relevant and proposed in several designs. In addition, chloride salts are being considered for MSRs operating in the fast neutron spectrum. This report focuses on chloride salts.

Fundamental molten salt thermodynamic and thermophysical properties (e.g., density, heat capacity, viscosity, and thermal conductivity) are important for the development of next-generation MSRs, in which molten salts are used as both coolant and fuel. However, due to the corrosive nature of molten salts, measurements of their properties at high temperatures can be experimentally challenging. This is even more pertinent for fuel salts, which, in addition, contain toxic and radioactive actinides (U, Pu) as fuel and after burnup a range of fission products, all of which may influence properties. Using atomic scale simulations to fill these data gaps and to provide mechanistic understanding of property relations would facilitate more accurate evaluation of various concepts by reactor designers, developers and other interested parties. Modeling and simulations have an important role to play in reducing data gaps, because the compositional space of interest is extensive and difficult to cover with experiments alone, especially since some of the salts are also highly toxic or radioactive. This benefit is already acknowledged in the literature [2–6], but the field is still evolving and many properties are either only partially explored or remains to be investigated, in particular for complex compositions.

In FY21, we have performed classical molecular dynamics (MD) and ab initio molecular dynamics (AIMD) simulations to predict the thermophysical properties of pure chloride salts and their mixtures in the $AlCl_3$-NaCl-KCl system over a wide temperature range from 800 K to 1400 K. Our classical MD simulations use a non-polarizable Buckingham pair potential in combination with a Stillinger-Weber three-body potential for Al-Cl-Cl interaction, which are parameterized using ab initio calculated data such as equilibrium lattice parameters and single-crystal elastic constants. MD predicted thermophysical properties are compared with experimental data when they exist. Our computational methods and results are summarized in this report. In addition, AIMD simulations relying on different models for Van der Waals interactions are used to predict temperature dependent thermophysical (density and thermal expansion) and thermodynamic (mixing energy and heat capacity) properties of NaCl, KCl and $AlCl_3$ mixed with $UCl_3$. Among these, the main topic for the FY21 milestone is $UCl_3$ mixed with KCl and $AlCl_3$, however, the NaCl study performed in previous years under NEAMS and lately for a different sponsor (LANL LDRD) provided the theoretical basis for the KCl and $AlCl_3$ studies. Consequently, this work will be reviewed to explain and provide justification for the simulation

methodology and to highlight the underlying chemistry and physics governing properties, as those are expected to be similar for at least the KCl-$UCl_3$ system. Classical potentials were not used for the actinide containing systems. For this reason thermal conductivity and viscosity are beyond the present scope.

This report is organized as follows. The first chapter is devoted to development of empirical potentials for KCl-NaCl-$AlCl_3$, applications and benchmarking of the potentials to a subset of thermodynamic and thermophysical properties in order to finally enable predictive simulations of complex properties such as of thermal conductivity and viscosity. This chapter also presents results of AIMD simulations used for benchmarking and a literature review of relevant experimental data. The final two chapters are devoted to AIMD simulations of actinide containing salts. First, the progress to-date on the NaCl-$UCl_3$ system is presented, which includes an introduction of the AIMD simulation methodology, identification of key results and lessons-learned. The next chapter extends the same methodology to KCl, $AlCl_3$ and KCl-$UCl_3$. The current state of results are compared and contrasted to the NaCl-$UCl_3$ system and available experimental data. Finally, we summarize our findings and present concluding remarks.

# 2 Empirical potential development and application for NaCl-KCl-$AlCl_3$

## 2.1 Methodology and potential parameters

Since the electronegativity value of Cl (3.16) is much larger than those of Na (0.93) and K (0.82), the chemical bonding in NaCl and KCl is predominantly ionic. In this study, we have employed a non-polarizable Coulomb-Buckingham [7] empirical potential that describes the pair interatomic interactions between ions $i$ and $j$ in NaCl and KCl salts as:

$$\phi_2(r_{ij}) = Z_i Z_j \frac{e^2}{r_{ij}} + A_{ij} e^{-\frac{r_{ij}}{\rho_{ij}}} - \frac{C_{ij}}{r_{ij}^6} \tag{2.1}$$

where $Z_i$ is the partial charge of ion $i$. The first, second, and third term on the right-hand side represent long-range Coulomb interaction, short-range repulsion interaction due to the overlap of the electron orbitals of two ions at small distances (Pauli repulsion), and attractive long-range van der waals dispersion interaction, respectively. The values for $C_{ij}$ are estimated in this work using the method of Grimme [8].

Compared with NaCl and KCl, the chemical bonding in $AlCl_3$ is much more complicated. While the electronegativity value of Cl (3.16) is still larger than that of Al (1.61), the difference is not large enough to form a simple ionic bond. In general, any ionic bond may also contain some partial covalent character due to the polarization of the electron cloud of an anion by neighboring cations. According to Fajans' rules, the degree of anion polarization will be more significant for cations with small sizes and high charges. Compared with the ionic radii of less charged $Na^+$ (1.02 Å) and $K^+$ (1.38 Å) ions, the ionic radius of $Al^{3+}$ (0.535 Å) is significantly smaller. The small size and high charge of the $Al^{3+}$ ion confer it with strong polarizing power. Consequently, $AlCl_3$ will also exhibit significant covalent bonding character.

In the solid state, $AlCl_3$ has a cubic Pm-3m structure (Figure 2.1a) in which each Al is coordinated by 6 Cl atoms. At around 180°C, $AlCl_3$ sublimes to form $Al_2Cl_6$ dimers, in which each Al is surrounded by 4 Cl atoms (Figure 2.1b). While Al and Cl atoms form strong covalent bonding within each $Al_2Cl_6$ dimer, the interactions between $Al_2Cl_6$ dimers are weak. With increasing temperature, a $Al_2Cl_6$ dimer will dissociate into two $AlCl_3$ molecules, and the coordination of the Al atom is further reduced to 3 (Figure 2.1c). Modeling such complicated phase transitions for $AlCl_3$ using an empirical potential will be a challenging task. In this work, we employ a Stillinger-Weber three-body term [9] for Al-Cl-Cl interaction to model the covalent character of Al-Cl bonding:

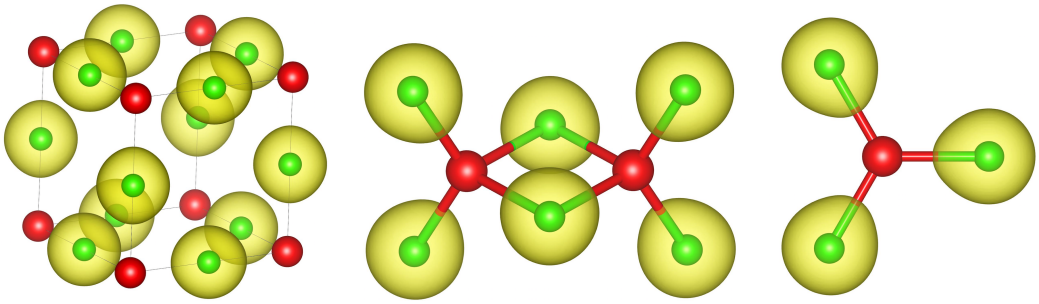

(a) Pm-3m (b) $Al_2Cl_6$ dimer (c) $AlCl_3$ monomer

Figure 2.1: Different structures of $AlCl_3$. Red and green spheres represent Al and Cl atoms, respectively.

$$\phi_3(r_{ij}, r_{ik}) = \lambda_{ijk}\left(\cos\theta_{ijk} - \cos\theta_0\right)^2 e^{\frac{\gamma_{ij}}{r_{ij}-a_{ij}}} e^{\frac{\gamma_{ik}}{r_{ik}-a_{ik}}} \tag{2.2}$$

where $\theta_0$ is set at 109.47°. The goal of adding this three-body term is to stabilize the $AlCl_4^-$ ions with a tetrahedral structure, which are known to exist in $AlCl_3$-NaCl and $AlCl_3$-KCl mixtures at the equiatomic composition [10, 11]. Due to the use of a fixed $\theta_0$, however, our model will not be able to describe the Pm-3m and monomer structures of pure $AlCl_3$, in which the Cl-Al-Cl bond angles are 90° and 120°, respectively.

We have fitted parameters $A_{ij}$, $\rho_{ij}$, $\lambda_{ijk}$, $\gamma_{ij}$, and $a_{ij}$ to the ab initio predicted properties of bulk crystals such as equilibrium lattice parameters and single-crystal elastic constants. The partial charges $Z_i$ have also been fine-tuned to give the best agreement with ab initio data. Density functional theory (DFT) calculations with PBE exchange–correlation functional have been performed using the Vienna ab initio simulation package (VASP) code [12]. Since local and semi-local density functionals such as PBE cannot describe van der Waals dispersion interactions, which is due to dynamical correlations between fluctuating charge distributions, we have employed the density-dependent energy correction (dDsC) method [13] for dispersion correction. A large plane-wave cutoff energy of 500 eV is used to ensure high numerical accuracy. The final optimized parameters for $AlCl_3$-NaCl-KCl salts are given in Tables 2.1 and 2.2 below.

Table 2.1: Pair interaction parameters for $AlCl_3$-NaCl-KCl system. $Z_{Al}$, $Z_{Na/K}$ and $Z_{Cl}$ are set at +2.7, +0.9 and -0.9, respectively.

| $i$-$j$ | $A_{ij}$ | $\rho_{ij}$ | $C_{ij}$ |
|---|---|---|---|
| Al-Cl | 4654.66 | 0.2778 | 76.66 |
| Na-Cl | 1480.98 | 0.3210 | 55.77 |
| K-Cl | 3166.25 | 0.3180 | 76.69 |
| Cl-Cl | 3081.71 | 0.3077 | 52.55 |

Table 2.2: Parameters for Al-Cl-Cl three-body interaction.

| *i*-*j*-*k* | $\lambda_{ijk}$ | $\gamma_{ij}$ | $a_{ij}$ |
|---|---|---|---|
| Al-Cl-Cl | 8.893 | 0.6 | 4.0 |

## 2.2 Classical molecular dynamics simulations

Using our developed empirical potentials, we have performed classical molecular dynamics (MD) simulations in the Large-scale Atomic/Molecular Massively Parallel Simulator (LAMMPS) [14] to predict the thermophysical properties of pure chloride salts and their mixtures in the $AlCl_3$-NaCl-KCl system over a wide temperature range from 800 K to 1400 K. For obtaining their equilibrium densities, heat capacities, and viscosities, periodic cubic simulation cell containing >13000 atoms are employed. At a given temperature, MD simulations in the NPT (constant number of atoms, pressure and temperature) ensemble are first performed to obtain the equilibrium lattice parameter. Long-time MD trajectories in the NVT (constant number of atoms, volume and temperature) and NVE (constant number of atoms, volume and energy) ensembles are then collected and used to extract heat capacities and viscosities, respectively.

Using Green-Kubo relation, viscosity can be obtained from equilibrium MD simulations via time integral of the off-diagonal terms of the stress autocorrelation function as:

$$\eta = \frac{V}{k_B T} \int_0^\infty \langle p_{xy}(0) p_{xy}(t) \rangle dt \tag{2.3}$$

where $V$ is volume, $p_{xy}$ is the off-diagonal component of the stress tensor, and $k_B$ is Boltzmann constant.

To compute thermal conductivities, the Muller-Plathe's reverse non-equilibrium MD method [15] is used, which induces a temperature gradient in a system by exchanging kinetic energy between atoms. Large supercells containing >110000 atoms that are elongated along the z axis are used for thermal conductivity calculations.

## 2.3 Ab initio molecular dynamics simulations

To validate our classical MD results, we have further performed AIMD simulations at $T$=800 K, 1000 K, 1200 K and 1400 K using the VASP code to obtain the equilibrium densities and specific heat capacities of pure chloride salts and their mixtures in the $AlCl_3$-NaCl-KCl system. Periodic cubic simulation cell containing >200 atoms are used to model molten salts. The dDsC method [13] is employed to account for the van der Waals dispersion interaction. A large plane-wave cutoff energy of 500 eV is employed. Due to the non-periodicity of the liquid state, a single $\Gamma$ point is sufficient for Brillouin zone sampling. The Newton´s equations of motion are numerically solved using Verlet´s algorithm with a time step of 2.0 fs. We employ a canonical (NVT) ensemble with a Nose-Hoover thermostat for temperature control. At a given temperature, the pressures of a simulation cell are calculated at 5 different volumes. At each volume, the system is first equilibrated for at least 5000 time steps, followed by a production run

with a duration of 5000 time steps. We obtain the pressure of a system from the time average of its AIMD production run trajectory. The pressure vs. volume data are then fitted to a Murnaghan equation of state (EOS) [16] to obtain the equilibrium volumes:

$$P(V) = \frac{B_0}{B_0^{'}} \left( \left( \frac{V_0}{V} \right)^{B_0^{'}} - 1 \right) \tag{2.4}$$

where $B_0$ is the bulk modulus and $B_0^{'}$ is its pressure derivative. $V_0$ is the equilibrium volume giving zero overall pressure. As shown in Figure 2.2, the Murnaghan EOS can describe the AIMD data with satisfactory accuracy. Importantly, adding $AlCl_3$ to pure NaCl and KCl salts significantly reduces their bulk moduli. For example, at $T$=1200 K, the bulk moduli of $NaAlCl_4$ and $KAlCl_4$ salts are calculated to be only 0.95 GPa and 0.62 GPa, respectively. For such low bulk moduli, the pressure will decrease rather slowly with increasing volume, and small errors in pressure calculations will lead to large uncertainties in the final calculated densities.

## 2.4 Structures of molten salts

Figure 2.3 shows the partial radial distribution functions (RDFs) for Na-Cl, K-Cl, Al-Cl, and Cl-Cl pairs in various molten salts in the $AlCl_3$-NaCl-KCl system at $T$=1400 K. It can be seen that our classical MD simulations using ab initio informed empirical potentials can adequately reproduce the cation-anion and anion-anion RDFs from AIMD simulations. The sharp first peak in Al-Cl RDF is due to the formation of stable $AlCl_4^-$ complexes in liquid $NaAlCl_4$ and $KAlCl_4$, as shown in Figure 2.4. The location of the first peak of Al-Cl partial RDF gives the average Al-Cl bond length to be $\sim$2.15 $\AA$ according to both AIMD and MD simulations. This predicted value is in excellent agreement with the experimentally measured nearest-neighbor distance between Al-Cl pair (2.13 $\AA$) from X-ray diffraction analysis [17].

A close examination of Figure 2.4 however reveals some discrepancies between AIMD and MD. While $AlCl_3$ monomers have been frequently observed in AIMD simulations, they are not formed during MD simulations due to the use of a Stillinger-Weber three-body term that favors $AlCl_4^-$ complex. Furthermore, during MD simulations of $NaAlCl_3$, a $Al_3Cl_{10}^-$ complex is formed due to the interconnection between $AlCl_4^-$ ions via corner sharing. Such large complexes have however not been observed in AIMD simulations. As will be discussed, the formation of long $Al_nCl_{3n+1}$ chain-like complexes in MD simulations will lead to an overestimation of viscosities.

## 2.5 Densities of molten salts

Figure 2.5 shows the calculated densities of various molten salts in the $AlCl_3$-NaCl-KCl system in comparisons with the experimental data from Janz [18], Van Artsdalen et al. [19], Berg et al. [20], and Andreasen et al. [21]. Overall, AIMD calculated equilibrium densities are in excellent agreement with the experimental measurements. In contrast, classical MD simulations tend to underestimate the densities, and such underestimation becomes more significant for $NaAlCl_4$ and $KAlCl_4$ salts due to their low bulk moduli.

## 2.6 Heat capacities of molten salts

Table 2.3 reports the AIMD- and MD-predicted specific heat capacities of various molten salts in the $AlCl_3$-NaCl-KCl system, which are obtained from linear fittings of total energy vs. temperature data at $T$=800 K, 1000 K, 1200K, and 1400 K. For NaCl, KCl, and their mixtures, classical MD simulations can predict their heat capacities within 11% of AIMD values. Due to the complex mixed ionic-covalent bonding between Al and Cl that is challenging to model by an empirical potential, our MD predicted heat capacities of NaCl-$AlCl_3$ and KCl-$AlCl_3$ salts can be up to 19% larger than AIMD results.

Table 2.3: Specific heat capacities of molten salts in the $AlCl_3$-NaCl-KCl system.

| **Salt composition** | **AIMD** | **MD** |
|---|---|---|
| NaCl | 1120 J/kg/K | 1246 J/kg/K |
| $Na_3KCl_4$ | 1074 J/kg/K | 1155 J/kg/K |
| $NaKCl_2$ | 1025 J/kg/K | 1095 J/kg/K |
| $NaK_3Cl_4$ | 986 J/kg/K | 1041 J/kg/K |
| KCl | 955 J/kg/K | 977 J/kg/K |
| $Na_3AlCl_6$ | 966 J/kg/K | 1147 J/kg/K |
| $NaAlCl_4$ | 920 J/kg/K | 1078 J/kg/K |
| $K_3AlCl_6$ | 910 J/kg/K | 1003 J/kg/K |
| $KAlCl_4$ | 833 J/kg/K | 994 J/kg/K |

## 2.7 Viscosities and thermal conductivities of molten salts

While the densities and specific heat capacities of a molten salt can be predicted using both MD and AIMD simulations, obtaining viscosity and thermal conductivity requires very long-time simulations (>1 ns) to achieve good statistical accuracy, which is computationally too demanding for AIMD. Therefore, only MD results for these properties are reported. As shown in Figure 2.6, MD predicted viscosities agree reasonably well with experimental data from Janz [18] and Ejima et al. [22]. For $NaAlCl_4$, however, there exist large discrepancies between MD simulations and experimental measurements by Cleaver and Koronaios [23]. Presumably, the formation of long $Al_nCl_{3n+1}$ chain-like complexes composed of $n$ corner-sharing $AlCl_4$tetrahedra (e.g. $Al_3Cl_{10}$ as shown in Figure 2.4b) will artificially strengthen the $NaAlCl_4$ liquid structure, which may contribute to explain the overestimation of viscosities by MD simulations. Note that $Al_nCl_{3n+1}$ complexes longer than $Al_2Cl_7$ have not been observed in our AIMD simulations.

As shown in Figure 2.7, the thermal conductivities for pure NaCl and KCl predicted by our non-equilibrium MD simulations are in good agreements with the experimental measurements by Nagasaka et al. [24] and the equilibrium MD simulations by Galamba et al. [25].

The composition-dependent viscosities and thermal conductivities for binary mixtures in the $AlCl_3$-NaCl-KCl system, as predicted by the present MD simulations, are shown in Figures 2.8 and 2.9, respectively. Importantly, it can be seen that adding $AlCl_3$ to pure NaCl and KCl salts

will significantly reduce their thermal conductivities, but will not drastically modify their viscosities. Note that the large increase of viscosity of a $(NaCl)_{1-x}(AlCl_3)_x$ salt with $x$ at $T$=800 K is most likely an artifact of the empirical potential used in our MD simulations, which leads to the formation of long $Al_nCl_{3n+1}$ chains at low temperatures. Finally, while the thermal conductivity of a $(NaCl)_{1-x}(KCl)_x$ salt will decrease with increasing KCl content, its viscosity is almost independent of $x$.

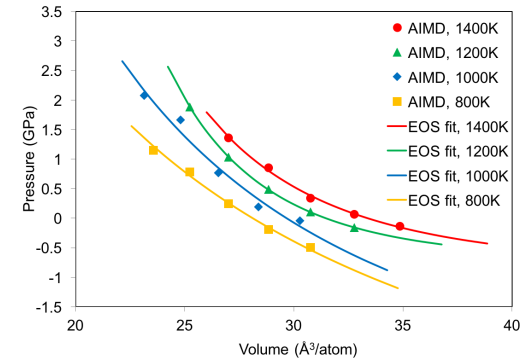


(a) NaCl

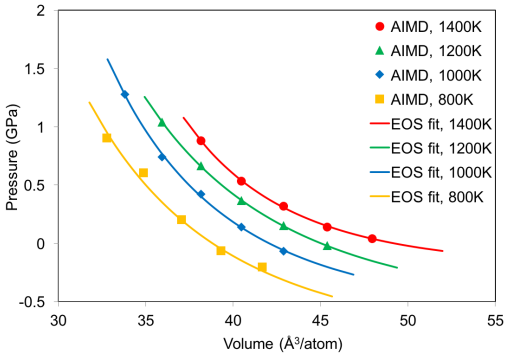


(b) KCl

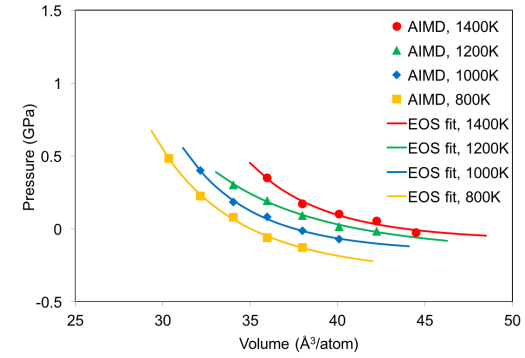


(c) $NaAlCl_4$

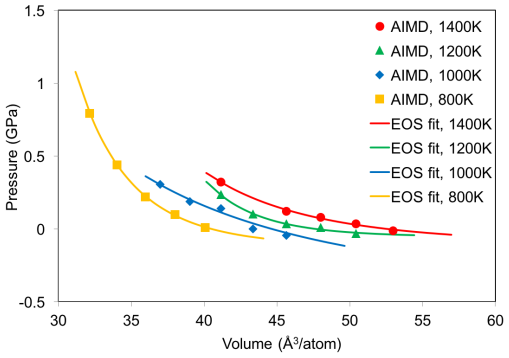


(d) $KAlCl_4$

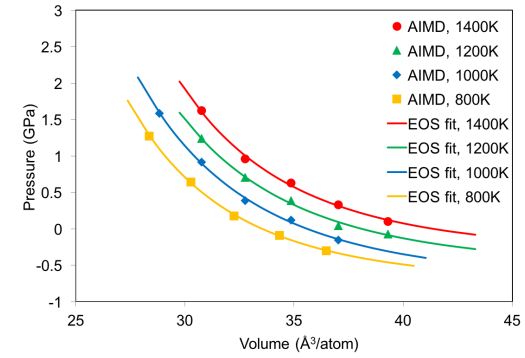


(e) $NaKCl_2$

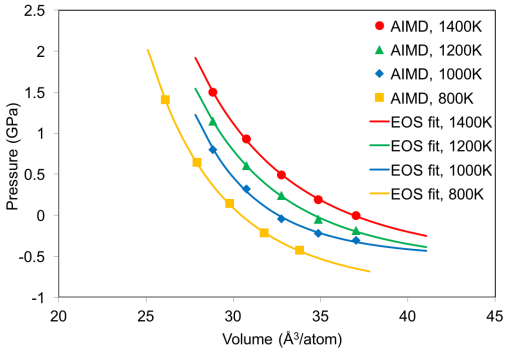


(f) $Na_3KCl_4$

Figure 2.2: Equation of state fitting of pressure vs. volume data from AIMD simulations.

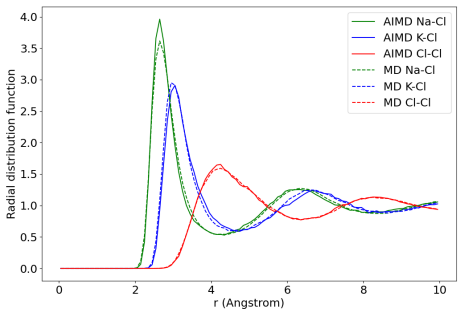


(a) $Na_3KCl_4$

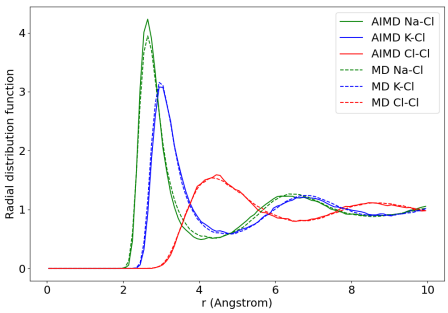


(b) $NaKCl_2$

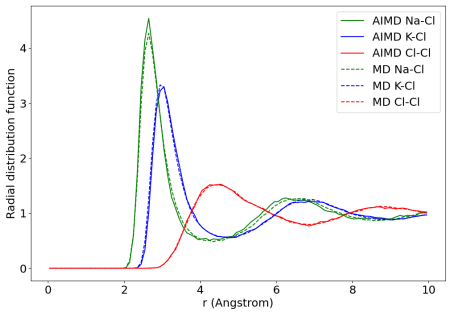


(c) $NaK_3Cl_4$

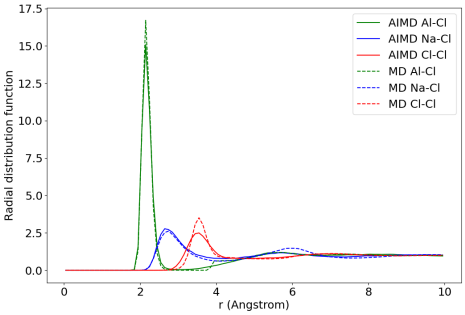


(d) $NaAlCl_4$

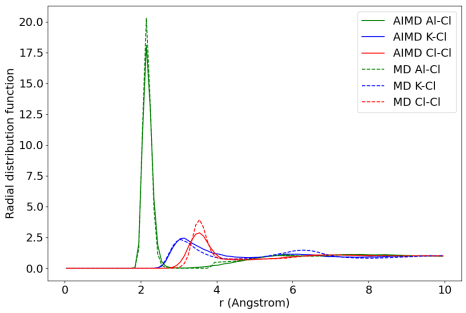


(e) $KAlCl_4$

Figure 2.3: Partial radial distribution functions of liquid $NaKCl_2$, $Na_3KCl_4$, $NaK_3Cl_4$, $NaAlCl_4$, and $KAlCl_4$ salts at $T$=1400 K from the present MD and AIMD simulations.

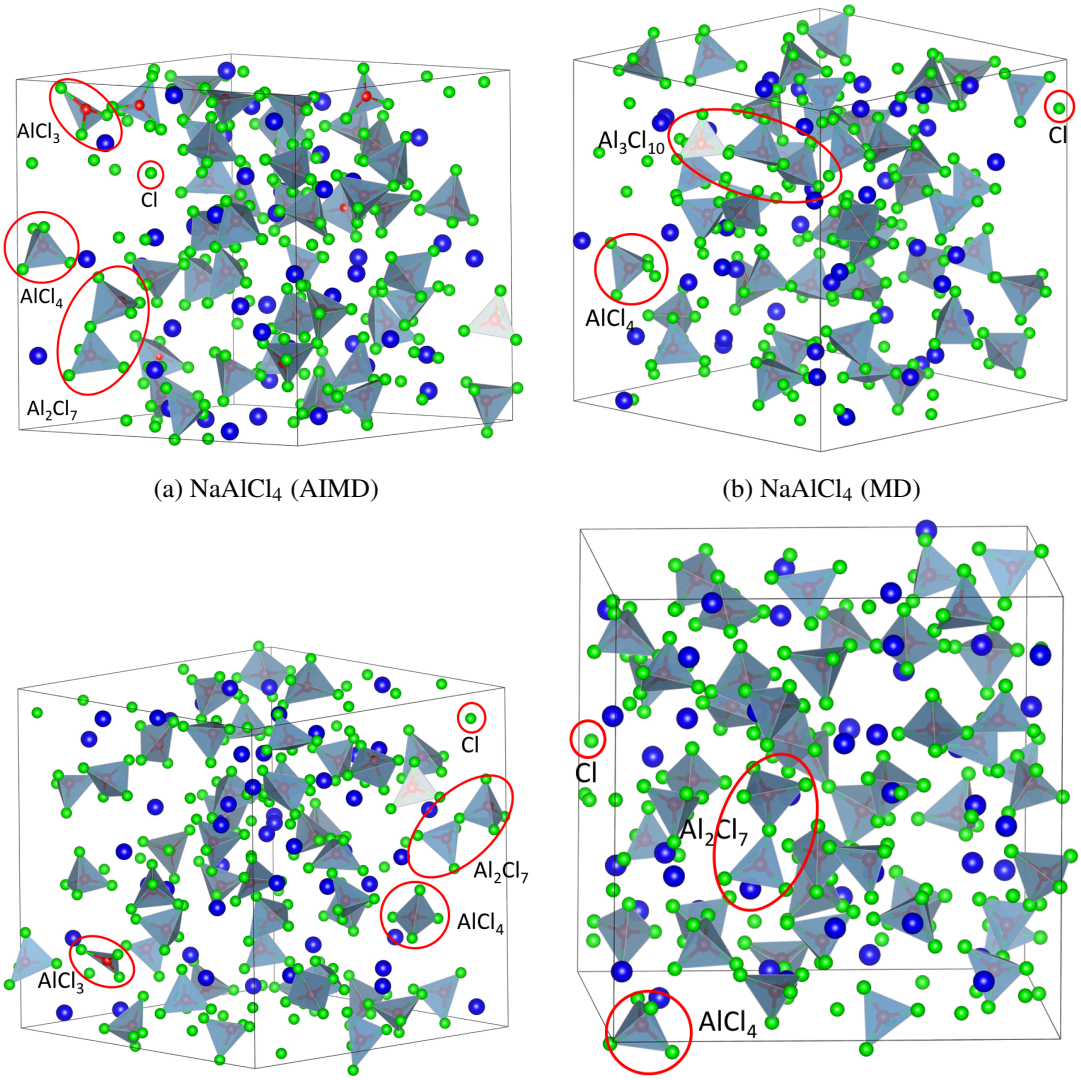


(a) $NaAlCl_4$ (AIMD)

(b) $NaAlCl_4$ (MD)

(c) $KAlCl_4$ (AIMD)

(d) $KAlCl_4$ (MD)

Figure 2.4: Snapshots of $NaAlCl_4$ and $KAlCl_4$ salts at 1400 K from AIMD and MD simulations. Red, green, and blue spheres represent Al, Cl, and Na/K atoms, respectively.

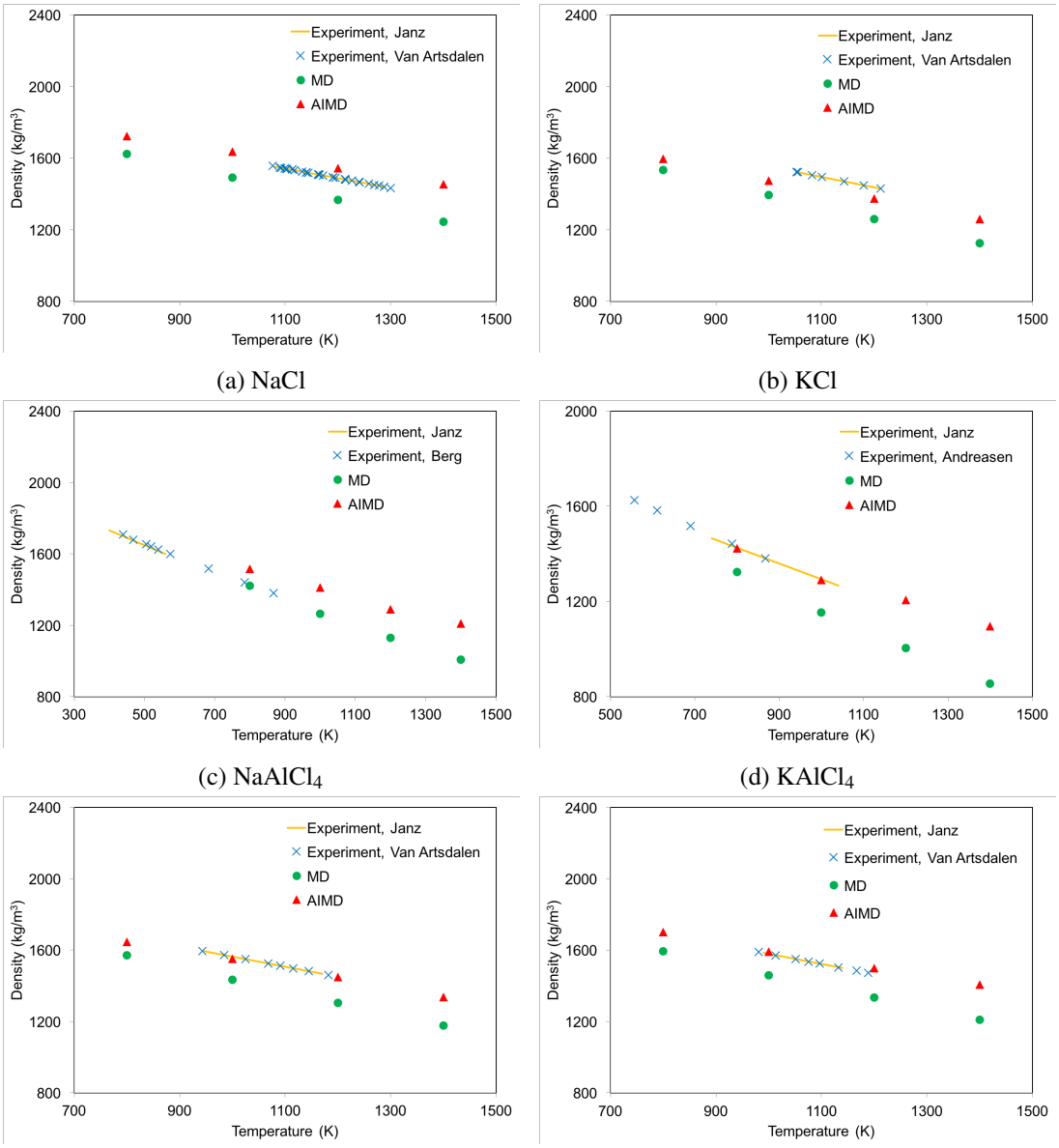


(a) NaCl




(b) KCl




(c) $NaAlCl_4$




(d) $KAlCl_4$




(e) $NaKCl_2$




(f) $Na_3KCl_4$

Figure 2.5: MD and AIMD predicted densities of molten salts in comparisons with experimental measurements.

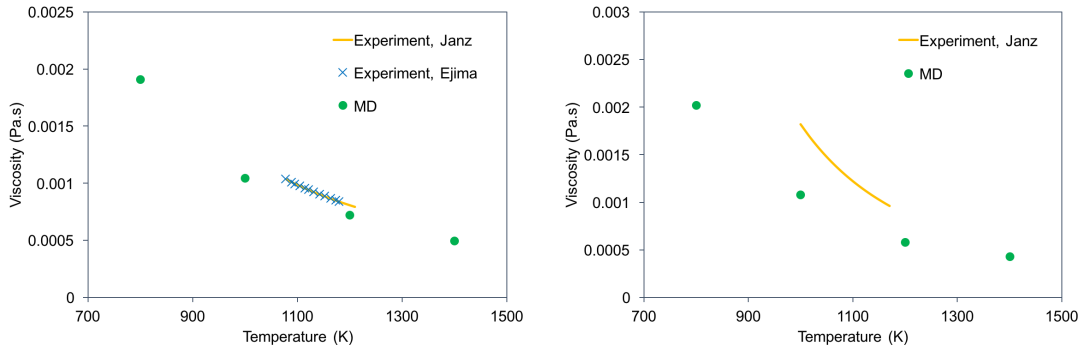


(a) NaCl




(b) $Na_3KCl_4$

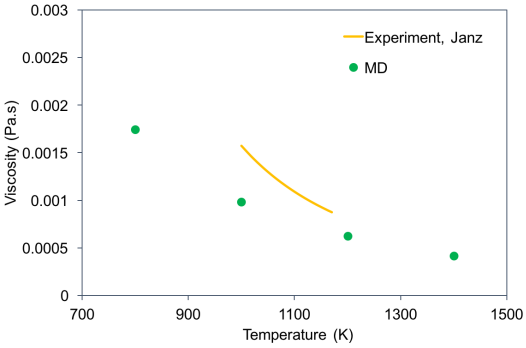


(c) $NaKCl_2$

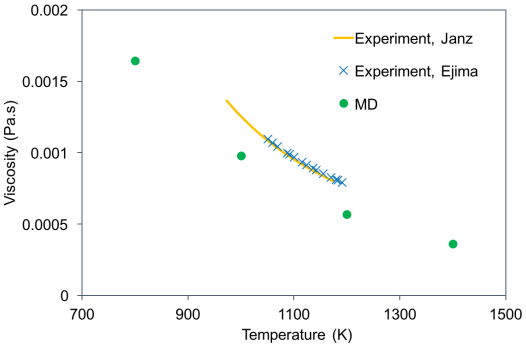


(d) KCl

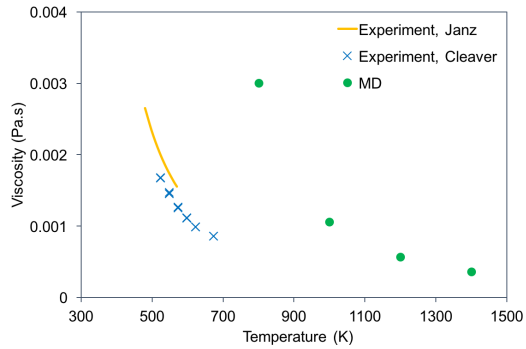


(e) $NaAlCl_4$

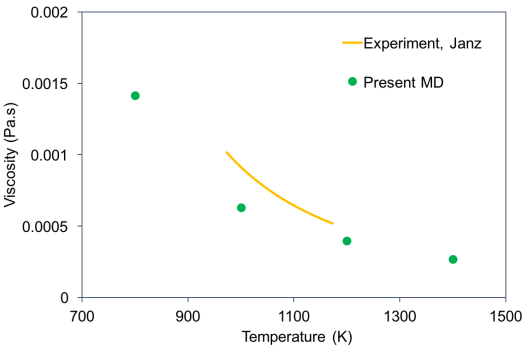


(f) $K_3AlCl_6$

Figure 2.6: MD and AIMD predicted viscosities of molten salts in comparisons with experimental measurements.

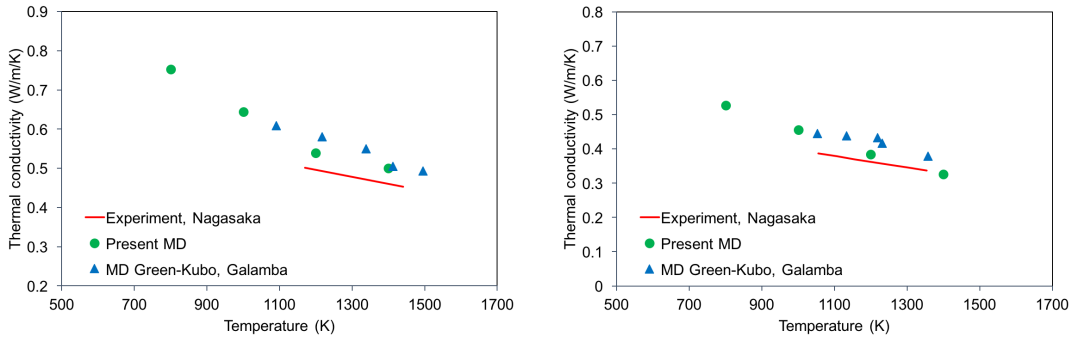


(a) NaCl (b) KCl

Figure 2.7: MD predicted thermal conductivities of NaCl and KCl in comparisons with experimental measurements.

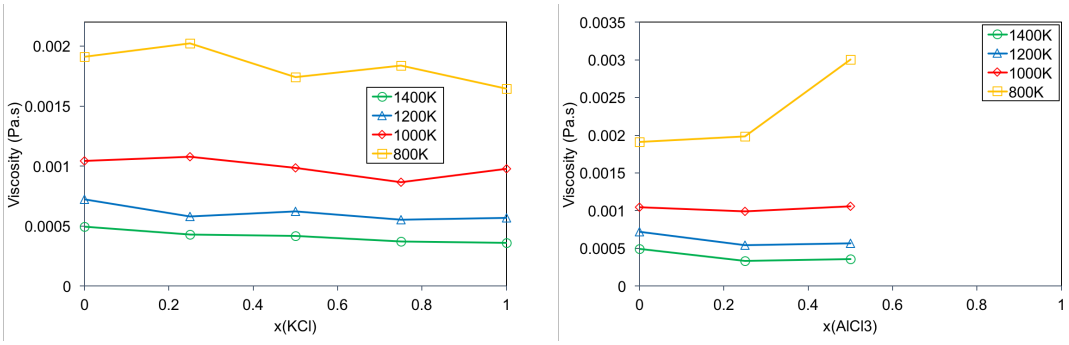


(a) NaCl-KCl (b) NaCl-$AlCl_3$

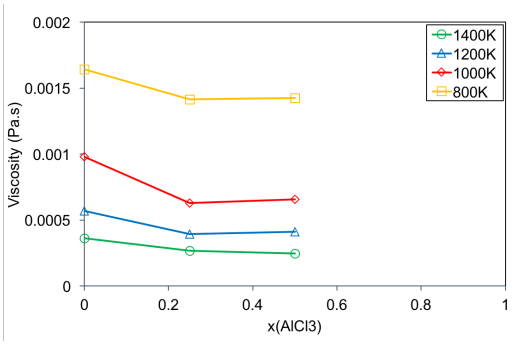


(c) KCl-$AlCl_3$

Figure 2.8: Composition-dependent viscosities in NaCl-KCl, NaCl-$AlCl_3$, and KCl-$AlCl_3$ systems predicted by the present MD simulations.

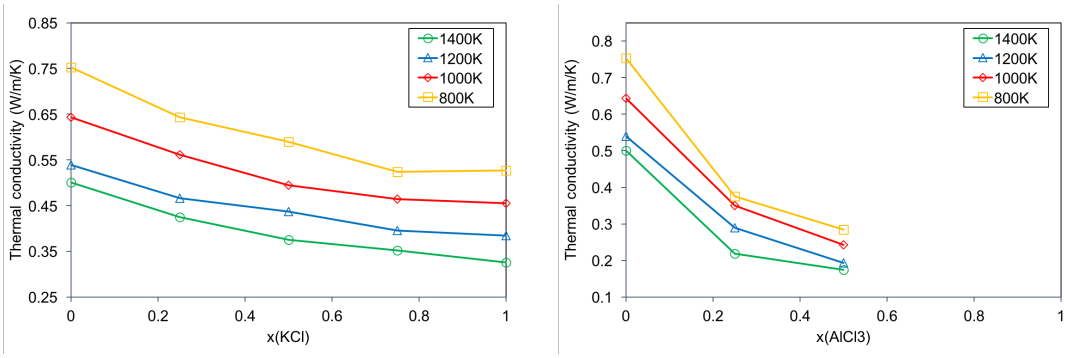


(a) NaCl-KCl

(b) NaCl-$AlCl_3$

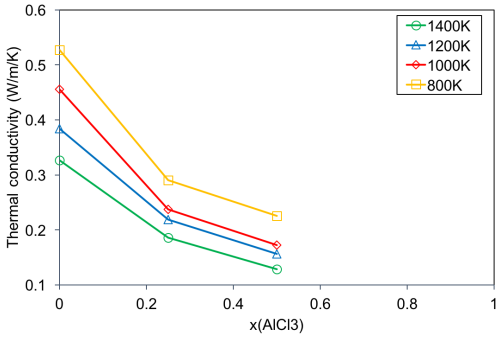


(c) KCl-$AlCl_3$

Figure 2.9: Composition-dependent thermal conductivities in NaCl-KCl, NaCl-$AlCl_3$, and KCl-$AlCl_3$ systems predicted by the present MD simulations.

# 3 Case study: Ab initio molecular dynamics simulations of select thermophysical and thermodynamic properties of NaCl, $UCl_3$ and NaCl-$UCl_3$ molten salts

The NaCl-$UCl_3$ system was the initial case study for applying AIMD simulations to actinide containing molten chloride salts, some of the work was performed under NEAMS in previous years (applications) and some under LANL LDRD (methods). The methodology established therein serves as the basis for the KCl-$UCl_3$ and $AlCl_3$-$UCl_3$ systems targeted in chapter 4. The simulation approach has continued to be refined as part of the present study. In order to introduce the methodology, understanding gained and lessons learned from studying the NaCl-$UCl_3$ system, the relevant details will be reviewed in this chapter.

## 3.1 Review of existing experimental and modeling studies on NaCl, $UCl_3$ and NaCl-$UCl_3$

Experimental characterization of $UCl_3$ densities have been reported by Janz et al. [18] and Desyatnik et al. [26]. The density correlations derived from these two experimental data sets deviate significantly from each other. Desyatnik et al. [26] also investigated the density of NaCl-$UCl_3$ mixtures. They identified a negative deviation from an ideal solution across most of the composition range, with the high-temperature $UCl_3$ region deviating slightly from this trend. Maatsura et al. [27] measured the mixing energies of NaCl-$UCl_3$ at 1173 K, which highlighted a negative deviation from ideal solution behavior, which implies an exothermic reaction, with a shallow minimum of $-0.07$ to $-0.08$ eV per formula unit close to the eutectic composition ($x_{UCl_3} \approx 0.35$), but perhaps slightly shifted towards the 50-50 composition. There are two Calphad assessments of the NaCl-$UCl_3$ system [28, 29]. The magnitude and shape of the NaCl-$UCl_3$ mixing energies are noticeably different between the two assessments [29]. The assessment by Benes et al. [28] arrived at a form with a minimum close to the eutectic composition ($x_{UCl_3} \approx 0.35$), while Yin et al. [29] used the experimental data due to Matsuura et al. [27] as input, which resulted in a more negative mixing energy that is shifted slightly closer to the 50-50 composition. The magnitude of the mixing energy is off by about 50% between the two assessments.

The sparse and sometimes contradictory experimental data on molten salts in general and the NaCl-$UCl_3$ system in particular provide justification for pursuing modeling and simulations as a complementary approach to gain improved understanding. This opportunity is already acknowledged in the literature. Molecular dynamics simulations based on both classical potentials and AIMD simulations have been used to study chloride salts involving actinides [2, 3, 5, 6]. Li et

al. [2] used AIMD simulations to study the local structure of $UCl_3$, $UCl_4$ and mixtures of $UCl_3$, $UCl_4$ and NaCl at 1173 K. This study showed good agreement with experiments for the radial distribution function of the first coordination shell and identified network formation of $UCl_3$ units in mixed NaCl-$UCl_3$ salts [2]. In order to study temperature dependent thermo-physical properties, a semi-empirical potential was developed [3]. This potential successfully predicted density, thermal conductivity and viscosity, though validation is challenged by the lack of experimental data. Nam et al. [5] studied the solution thermodynamics of dilute concentrations of $UCl_3$ in a base salt and investigated the properties of base salts for different Van der Waals interaction models. Song et al. [6] performed AIMD simulations of densities and transport properties in a LiCl-KCl eutectic salt with a small concentration of $UCl_3$.

In the present study, AIMD simulations relying on different models for the Van der Waals interactions were used to predict temperature dependent thermophysical (density) and thermochemical (mixing energy and heat capacity) properties of NaCl, $UCl_3$ and NaCl-$UCl_3$. The standard PBE exchange-correlation potentials typically used were extended to include a Hubbard $U$ model for the actinide 5f electrons. The purpose of the study was first to determine with what accuracy fundamental properties can be predicted with AIMD simulations for actinide containing salts, second to populate some of the data gaps that exist in the literature and third to provide understanding of the link between coordination chemistry and properties.

The next sections are organized as follows. The methodology is described in Sec. 3.2, followed by results and discussion in 3.3. First the benchmark for NaCl is presented, next the $UCl_3$ results are reviewed, which is followed by NaCl-$UCl_3$ mixtures. The connection of our results to local chemistry and pair distribution functions are discussed in Sec. 3.4.

## 3.2 Methodology

The AIMD simulations were performed with the VASP code [12]. The simulations used a range of supercell sizes with the largest consisting of 216 (NaCl), 216 ($UCl_3$) and 134-184 (NaCl-$UCl_3$ mixtures) atoms. The smallest cells for the same systems contain 64, 64 and 60-72 atoms, respectively. For NaCl and $UCl_3$ these were created by expansion of the crystalline unit cells followed by melting of the lattice by performing high temperature MD simulations. The mixed supercells were created by replacing Na ions with U ions or vice versa, in some cases additional molecular units were added to ensure that an suitable number of atoms were maintained in the supercells. The differently sized supercells were investigated in order to understand and optimize the compromise between computational efficiency, enabling sampling in the time domain, and accuracy with respect to long range interactions. The radial distribution function (RDF) was used as the most basic measure of the adequacy of the supercell size, with convergence with respect to the targeted thermophysical and thermodynamic properties following suite. All the supercells investigated properly capture the expected radial distribution function in the liquid state. This behavior is exemplified in Figures 3.1a) and 3.1b) for two $UCl_3$ and NaCl supercells of different size, respectively. The smaller cells predict essentially identical radial distribution functions to the larger cells, but come with improved computational efficiency. Although the larger cells may still be more accurate for, e.g., mixed salts exhibiting more complex radial distribution functions, the situation in mixed salts is further complicated by the need to sample

sufficient configurations to resolve the preferred short and intermediate range distribution of ionic species in network forming salts such as $UCl_3$ [2]. This requires fairly long simulation times. Proper sampling is easier to achieve in smaller supercells given the computational cost of AIMD simulations, even though the radial distribution itself as well as other properties may be better described in a larger supercell. For this reason, our production runs tend to use supercells of intermediate size. Based on the verification against large supercells for the radial distribution function above and further examples in Sec. 3.3, the results in the present study are considered sufficiently converged with respect to supercell size.

All simulations used the $\Gamma$ point for integration in reciprocal space. The accurate simulation setting was utilized in VASP, but the plane wave cut-off energy was increased above the standard setting to 400 eV. Gaussian smearing with a smearing parameter of 0.05 eV was used for the partial occupancies of the wave functions. The convergence criteria for the electronic minimization was at least$10^{-3}$ eV for NaCl and $5 \times 10^{-3}$ eV for salts containing uranium.

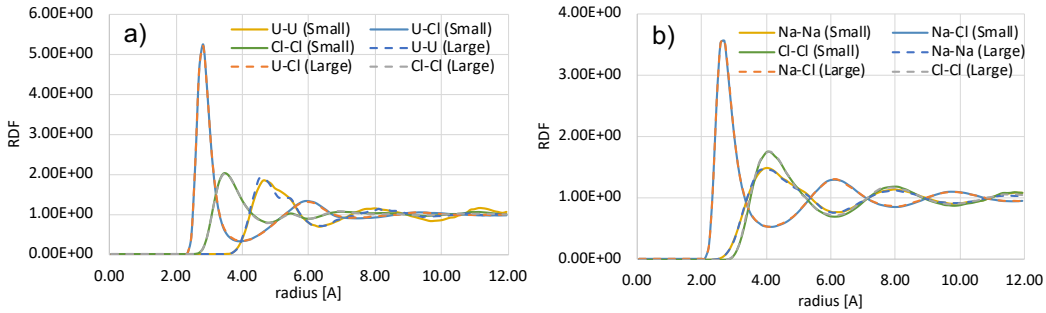


Figure 3.1: The predicted radial distribution function in a) $UCl_3$ and b) NaCl obtained by supercells containing 64 (small) and 216 (large) atoms at 1250 K.

The Projector Augmented Wave (PAW) method was used to describe the core electrons [30, 31]. For each element, the PAW potentials supplied with VASP for the PBE exchange-correlation potential were utilized. For Na, the version that only includes the s electron(s) in the valence shell was used. The PAW potential for Cl also included p electrons and for U it included the outer s, p and f electrons in the valance shell. Calculations for U ions were performed with a Hubbard $U$ term, in order to capture the impact of accounting for strong electron correlation effects. The Lichtenstein approach [32] was used for the Hubbard $U$ methodology. An approximate $U$ value range of 3.0-4.5 eV was determined by using scoping constrained DFT linear-response method for crystalline $UCl_3$ [33]. The $J$ value was set to 0.51 eV. These values are similar to those proposed for $UO_2$ [34]. After confirming that the values for $UCl_3$ were close to those for $UO_2$, the values for $UO_2$ were adopted in the present study. Future work may consider further optimization of the Hubbard $U$ (and $J$) parameters, but the results and conclusions are not expected to significantly change based on this choice, as long as the value is sufficiently large to ensure an insulating ground state. It should be noted that the effective $U$ value depends on the coordination environment and consequently could differ between crystalline $UCl_3$ and molten salts. It could also be a function of time in the simulations as the environment may change. Future work may consider these questions in more detail, but it is beyond the scope of the present study. The effect of the Hubbard $U$ parameter for molten uranium chloride salts is the

same as for crystalline $UO_2$; without the $U$ parameter the salts are predicted to be metallic, which is contrary to the expected behavior. Even though useful results may certainly be obtained while ignoring the strong correlations captured by the Hubbard $U$ model and accepting the resulting metallic character predicted for the salts, there are limitations to this approach. For reference, a few simulations were performed without the Hubbard $U$ model (not shown).

Uranium ions in its 3+ state have localized magnetic moments. In order to mimic the disordered arrangement of magnetic moments expected at temperatures where the salts are molten, the spins were arranged in an anti-ferromagnetic (AFM) pattern and then allowed to relax during the simulations. In the context of molten salts, the AFM option is similar to a random distribution with a total magnetic moment in the supercell close to zero. The predicted properties are not strongly influenced by the magnetic ordering.

It is well-established in the literature that Van der Waals or dispersion interactions are critical for reproducing the density of molten salts by DFT methods [2, 4, 5]. Previous simulations have used both the DFT-D3 method [2, 35] and the Langreth & Lundqvist [5, 36, 37] methodologies for various molten chloride salts. Both methods were used in the present study, although the Langreth & Lundqvist method was dropped after concluding that it was not very accurate for pure $UCl_3$. In addition, the density-dependent energy correction (dDsC) method [13, 38] was used with the goal of improving accuracy. The dDsC method does not include parameters for f elements in the standard VASP version. In order to enable simulations the corresponding parameters were taken from Ref. [39].

The AIMD simulations for the molten salt supercells were performed using isobaric conditions (NPT) conditions. The primary intent of the NPT simulations (with the pressure set to zero) is to evaluate density, thermal expansion, heat capacity and mixing energy. All NPT ensemble simulations used the the Langevin thermostat in VASP. For the NPT simulations, the temperature friction coefficient was set to 10 $ps^{-1}$ and the friction coefficient for the lattice degrees of freedom to 1 $ps^{-1}$. The time step was set to 2 fs for production runs between $\tilde{1}$000 K and 1500 K. Around and below 1000 K a larger time step, up to 5 fs, is warranted due to the slow dynamics of uranium ions. In principle, the larger time step can also be applied at higher temperatures as long as the structures have been properly converged.

The simulations used pre-equilibrium and equilibration runs that involve melting the lattice and ensuring convergence of the total energy and pair distribution function for the temperature of interest. After pre-equilibration and equilibration, production runs follow for at least 20 ps. Some simulations used longer production runs, in particular this applies to the simulations based on smaller supercells (up to 50 ps) and systems containing a mixture of $UCl_3$ and NaCl (up to 40 ps). NPT simulations often require long equilibration runs and may sometimes leave the equilibrium state due to distortions of the supercells. All simulations were inspected to avoid sampling such regimes.

Properties were calculated by averaging over the production run (not including the equilibration or pre-production time). Densities were trivially obtained from the supercell volume and heat capacities from the slope of the total internal energy ($E_{tot}$) as function of temperature.

$$C = \frac{\partial E_{tot}}{\partial T} \tag{3.1}$$

For the NPT ensemble, this corresponds to heat capacity at constant pressure ($C_p$). Mixing

energies were calculated from the potential energy ($E_{pot}$) of the mixed salt with pure NaCl and $UCl_3$ at the same temperature as the reference.

$$E_{mix} = E_{pot}(U_xNa_yCl_{3x+y}) - xE_{pot}(UCl_3) - yE_{pot}(NaCl). \tag{3.2}$$

## 3.3 Results

### 3.3.1 Ab initio molecular dynamics simulations on NaCl

#### Density and structure

Figure 3.2a plots the predicted density of molten NaCl as function of temperature for the DFT-D3 and DFT-dDsC Van der Waals models as well as simulations without any dispersion interaction. The results refer to the supercell size that we consider best converged for each methodology, see caption and below for further discussion. A correlation derived from experimental data is also shown [18]. All simulations reproduce the temperature dependence of the density obtained from experiments. However, as expected, only the simulations that account for dispersion interactions are within 10% of the experimental density correlation. The best agreement is obtained for the dDsC dispersion model, which is within 5% or less of the experimental correlation across an extended temperature range. The calculated (dDsC) correlation for the density as function of temperature is listed in Table 3.1. The radial pair distribution function at 1250 K is reported in Figure 3.1, which highlights first, second and third-shell coordination distances of 2.70 Å, 3.78 Å and 4.14 Å, respectively. The predicted pair distribution function is in good agreement with experimental values [40].

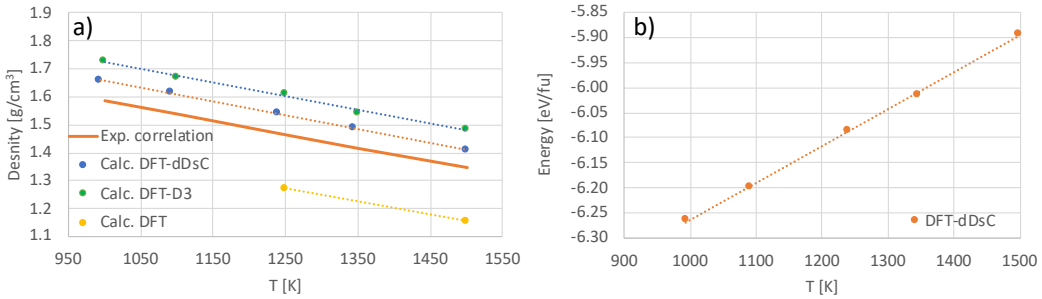


Figure 3.2: a) Density of NaCl predicted with two different models for dispersion forces (D3 and dDsC) and one without (small cell for dDsC, large cell for others). Experimental data is represented by the correlation plotted as an orange line [18]. b) Calculated total energy of NaCl as function of temperature (small cell). The line is a least-squares fit to data points and the slope represents the heat capacity.

#### Heat capacity

Figure 3.2b plots the total energy per formula unit of molten NaCl as function of temperature. The derivative equals the heat capacity of NaCl, which is also tabulated in Table 3.1 together

with an experimental reference value [41]. The results refer to the supercell size that we consider best converged for each methodology, see caption and below for further discussion. The simulation results indicate a constant heat capacity, though in order to identify small deviations from this behavior a denser temperature mesh would be required. The good agreement between simulations and experiments for the heat capacity (see Table 3.1) further emphasizes the accuracy of the AIMD simulations.

### Impact of supercell size and other simulation settings

The results in Figure 3.2 refer to simulations based on the supercell that we consider best converged. Figure 3.3 compares these results with those obtained from other supercells. Density and heat capacity are accurately represented by all supercell sizes in the temperature range investigated. These results suggest that for NaCl, the larger supercell is not required to achieve converged results for density and heat capacity at moderate temperature, which is consistent with the discussion of radial distribution functions in Sec. 3.2. The small variations between supercells are more likely related to sampling differences, rather than due to the supercell size. Consequently, the converged results in Figure 3.2 as well as the correlations in Table 3.1 are representative of all simulation results in this study, regardless of the supercell size.

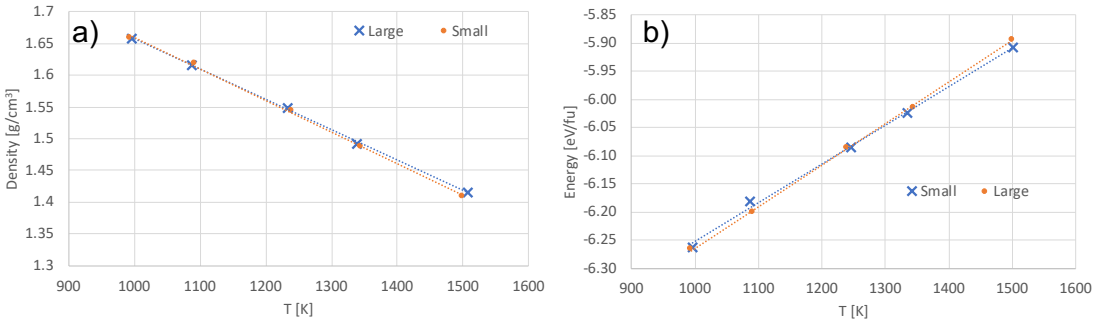


Figure 3.3: a) Calculated density and b) total energy of NaCl as function of temperature for the large and small supercells. The lines are least-squares fits to data points and the slope represents the heat capacity.

| | Density (g/cm$^3$) | Heat capacity (J/mol/K) |
|---|---|---|
| NaCl Calculated (dDsC) | $2.1594 - 0.0004993T$ | 71.6 |
| NaCl Experiment | $2.061 - 0.0004759T$ [18] | 66.9 [41] |
| $UCl_3$ Calculated (dDsC) | $6.1066 - 0.001383T$ | 145.3 |
| $UCl_3$ Experiment | $6.375 - 0.001522T$ [26] | 150 [42] |

Table 3.1: Calculated and experimental correlations and values for density and heat capacity of NaCl and $UCl_3$.

### 3.3.2 Ab initio molecular dynamics simulations on $UCl_3$

#### Density and structure

Following the results for NaCl, the best performing Van der Waals model (dDsC) was applied to $UCl_3$. Figure 3.4a) plots the predicted density for $UCl_3$ as function of temperature for the dDsC dispersion model. These results refer to the supercell size that we deem to be best converged and most representative of the $UCl_3$ system, see below for further discussion. The figure also compares the predicted densities to two literature correlations derived from experiments [18, 26]. The two experimental correlations for density are surprisingly different and cannot both be correct, except in a narrow temperature range. The temperature dependence is predicted to be close to linear across the full temperature range investigated and agrees very well with the experimental data due to Desyatnik et al. [26]. The densities in Figure 3.4 were fitted to linear correlations and summarized in Table 3.1.

The radial pair distribution function at 1250 K is reported in Figure 3.1, which highlights a first-shell coordination distance of 2.82 Å. The coordination distance is in excellent agreement with the experimental values of 2.82 Å [43] and 2.84 Å [44] measured at 1113 K and 1200 K, respectively, while it is higher than the AIMD simulations by Li et al. [2], which can likely be ascribed to the application of the Hubbard $U$ methodology in the present study. The predicted coordination numbers are within the 6 to 8 range reported in experiments and previous simulations [2, 43, 44].

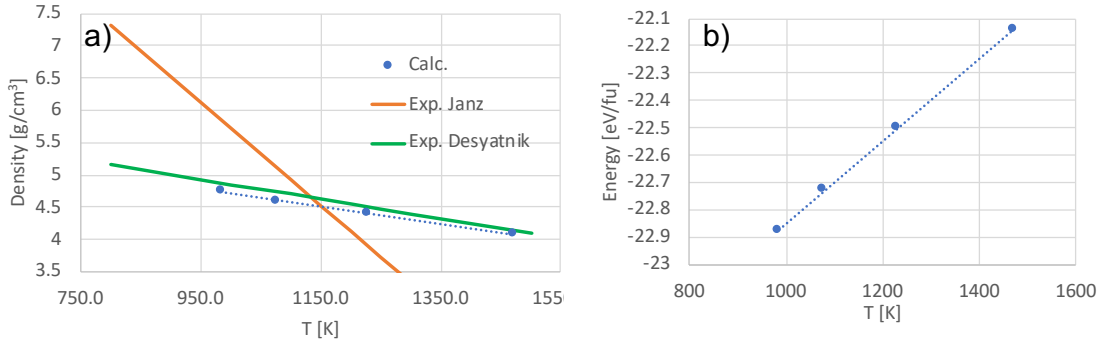


Figure 3.4: a) Density of $UCl_3$ predicted the dDsC model for the dispersion forces (small cell). Experimental data is represented by the correlations plotted as green [26] and orange lines [18]. The dashed line is a least-squares fit to the calculated data points, the equations of which are summarized in Table 3.1. b) Calculated total energy of $UCl_3$ as function of temperature (small cell). The line is a least-squares fit to data points and the slope represents the heat capacity.

#### Heat capacity

Figure 3.4 plots the total energy as function of temperature, from which the heat capacity can be derived by calculating the slope. The total energy closely follows a linear relation as function of temperature and, consequently, the heat capacity can be approximated as a constant in the temperature range investigated. In order to resolve small deviations from the linear relation, a

denser temperature mesh would have to be used. Experimental data for the heat capacity of $UCl_3$ has not been identified, but our results compare very well with the value derived from the MSTDB CALPHAD assessment of the $UCl_3$ thermodynamics (see Table 3.1) [42].

#### Impact of supercell size and other simulation settings

The results discussed above for $UCl_3$ refer to simulations using the supercell size that we deem to be best converged and most representative of the $UCl_3$ system for each simulation methodology. Select results obtained from different supercell sizes are compared in Figure 3.5, which exhibits fairly good agreement with each other. Any difference between supercell sizes is primarily ascribed to sampling appropriate configurations rather than an effect of increasing the numbers of ions in the simulation box, although additional simulations would be required to fully certify this conclusion. Compared to NaCl it is much more challenging to reach long simulation times for the large $UCl_3$ simulation cells.

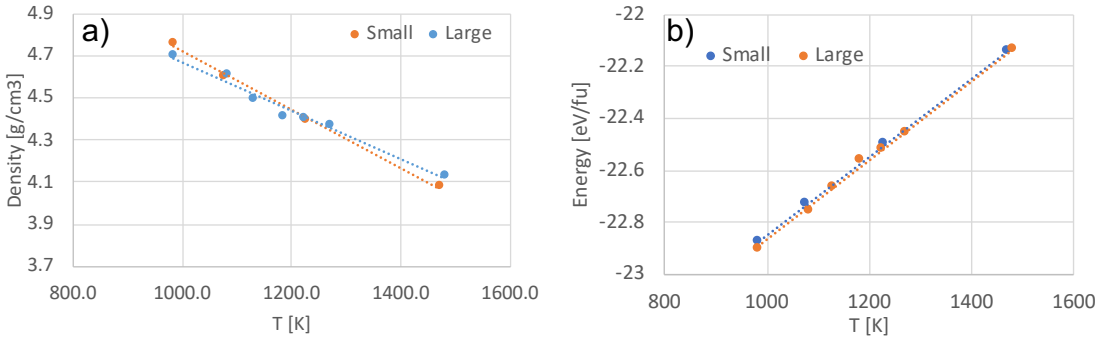


Figure 3.5: Calculated density and total energy of $UCl_3$ as function of temperature for the large and small supercells. The line is a least-squares fit to data points and the slope represents the heat capacity.

### 3.3.3 Ab initio molecular dynamics simulations on NaCl-$UCl_3$

#### Density and structure

The density of NaCl-$UCl_3$ mixtures were calculated for the dDsC dispersion model at three or four (depending on composition) different temperatures between 800 K and 1500 K, as shown in Figure 3.6a). This figure also includes densities at the same temperatures as those of the simulations obtained from correlations derived from experimental data due to Desyatnik et al. [26]. Figure 3.6b) highlights the fractional deviation from ideal solution behavior as calculated from simulations and experiments [26]. It is challenging to converge the density for mixed salt solutions to an accuracy better than around one per cent of the absolute density using AIMD simulations, which gives rise to some scatter in the data points. Nevertheless, a few trends are discernible from Figure 3.6. The simulated data points are within a few per cent of the experimental data. The simulations suggest a negative deviation from an ideal solution (lower density than predicted by an ideal solution behavior) by up to 2-3%, except close to pure $UCl_3$ at high

temperature where a positive deviation is observed. According to our simulations, the magnitude of the deviation from ideal solution behavior is a function of composition and varies some with temperature starting at $x_{UCl_3} \approx 0.35$ and continuing in the $UCl_3$ rich composition range, while it is almost independent of temperature in the NaCl rich range. The maximum deviation from ideal solution behavior occurs close to the eutectic composition of 35% $UCl_3$. These predictions are qualitatively similar to the correlations derived form experiments by Desyatnik et al. [26], though the experimental correlations predict a larger magnitude for the deviation from an ideal solution and also exhibit a stronger temperature dependence than the simulations.

Figure 3.7a) plots the density as function of temperature for each composition, which emphasizes a close to linear temperature dependence, similar to the pure end-members. The coefficients describing the linear dependence on temperature for each composition are plotted in Figure 3.8a). Although there is some scatter, a weak non-linear dependence on composition for both the linear and constant term (not shown) is identified. The non-linear dependence is most pronounced in the $UCl_3$ rich range. The density correlations identified in Figures 3.7a) and 3.8a) can, in principle, be used for calculating densities at temperatures and compositions not explicitly investigated by AIMD simulations.

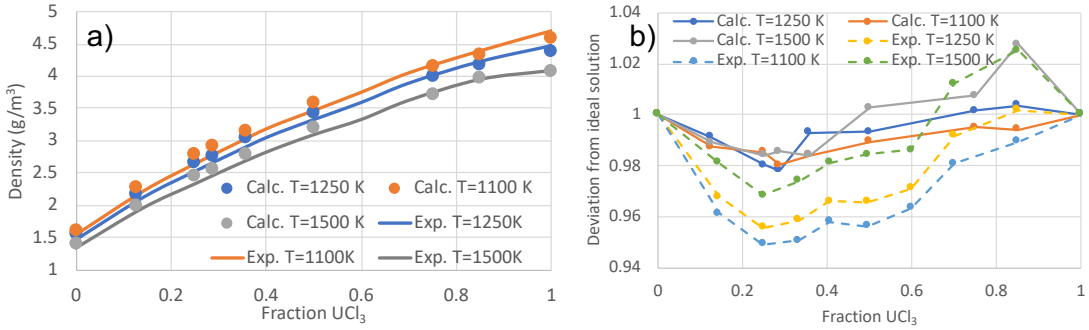


Figure 3.6: a) Density of NaCl-$UCl_3$ mixtures as obtained from simulations and experimental data [26] at temperatures between 1100 K and 1500 K. b) The fractional deviation form ideal solution behavior plotted as function of composition at temperatures between 1100 K and 1500 K.

### Mixing energy and heat capacity

The mixing energies of NaCl-$UCl_3$ at temperatures ranging from 1100 K to 1500 K are plotted in Figure 3.9a), with the NaCl and $UCl_3$ end members as reference points. The mixtures exhibit a negative deviation from ideal solution behavior, which implies that the solution phase is favored over a two-phase mixture of the end-points. Addition of entropy further stabilizes the mixed solution phase, as shown in Figure 3.9b) by adding a simple ideal solution model to the potential energy in Figure 3.9a). The minimum (most negative) mixing energy is between $x_{UCl_3}$=0.35 and $x_{UCl_3}$=0.5, which qualitatively mimics the results for the density.

The mixing energy was measured at 1100 K by Matsuura et al. [27] The results are also shown in 3.9a) and indicate very good agreement with the simulations across the full temperature range. In addition to the experimental data points, there are two sets of thermodynamic

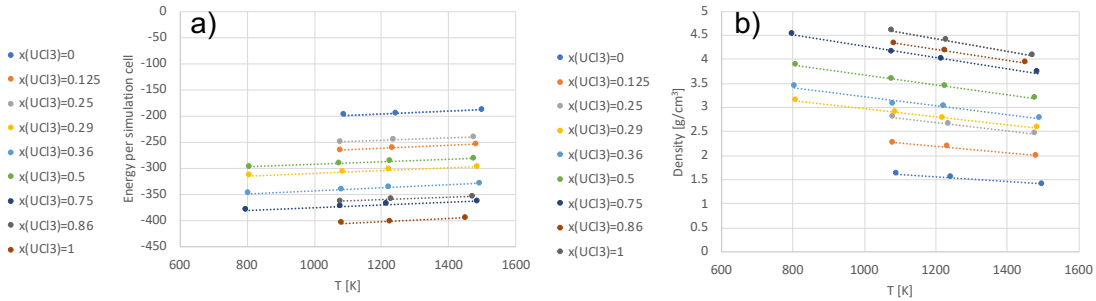


Figure 3.7: a) Calculated temperature dependent densities as function of composition. b) Calculated energies per simulations cell as function of composition. In both a) and b) the lines represent least-squares fits to the calculated data.

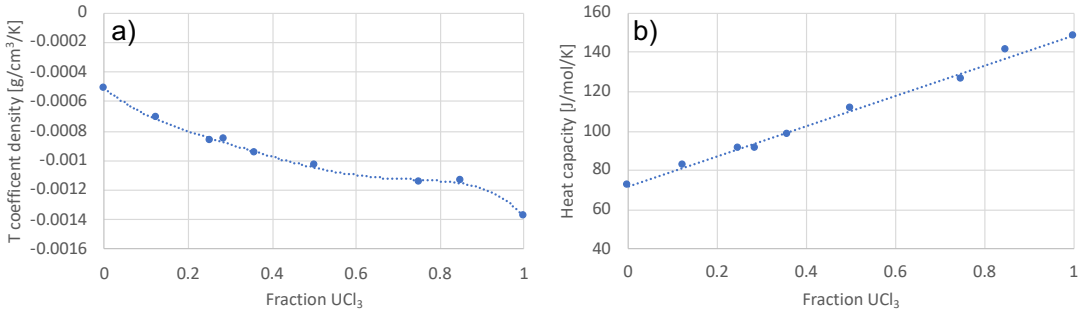


Figure 3.8: a) Coefficient describing the linear temperature dependence of density as function of the $UCl_3$ fraction. The line represents a least-squares fit of a fifth order polynomial. b) Heat capacity as function of the $UCl_3$ fraction. The line represents a least-squares fit of a linear correlation.

models for the solution energy [28,29], see Figure 3.9a) for the correlation from Ref. [29]. Both thermodynamic models assume the solution energy to be independent of temperature, which is in good agreement with the simulations. The model by Yin et al. [29] was derived from the experimental measurements by Matsuura et al. [27] and consequently agree similarly well with our simulation results. The model by Benes et al. [28] exhibits a smaller mixing energy than both the experimental data points and our simulations (not shown).

The total energy for each NaCl-$UCl_3$ composition is plotted as function of temperature in Figure 3.7b), from which heat capacity can be calculated as the slope, similar to the pure NaCl and $UCl_3$ systems. The heat capacity is a linear function of the salt composition, which is expected based on the lack of temperature dependence for the salt mixing energies. The negative deviation from an ideal solution seen for the mixing energy and density is not present for the heat capacity.

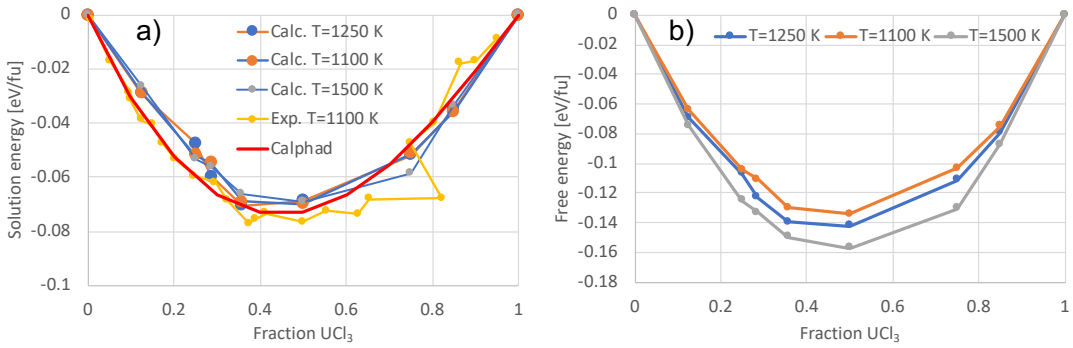


Figure 3.9: a) Mixing energies for NaCl-$UCl_3$ at 1100, 1250 and 1500 K. Pure NaCl and $UCl_3$ are used as references. The calculated results are compared to experiments [27] and a thermodynamic assessment [29].Results are shown for the best converged supercells. b) The free energy of mixing at 1100 1250 and 1500 K assuming an ideal solution.

## 3.4 Discussion

This discussion section will focus on the behavior of mixed salts, in particular how the mixing properties (energy and density) relate to the evolution of the pair distribution functions in the mixed salts. Figure 3.10 plots the pair distribution functions at four salt compositions ($x_{UCl_3} = 0.25$, $x_{UCl_3} = 0.29$, $x_{UCl_3} = 0.36$ and $x_{UCl_3} = 0.50$) and compares them to the reference pair distribution functions for $UCl_3$. Ref. [2] already showed that as NaCl is added to pure $UCl_3$, the number of Cl ions in the first neighbor shell around U ions increases, from 6 in $UCl_3$ to almost 8 close to NaCl, with a corresponding decrease around Na ions. This is also confirmed in the present study (see the increase of the first peak in Figure 3.10 as the NaCl fraction increases). This redistribution of Cl ions clearly represents a favorable interaction as the mixing energy is negative across the full composition range. The same study also identified networks of $UCl_3$ units above a fractional $UCl_3$ concentration of 0.30, and more isolated units below this concentration. This behavior is also visible in the pair distribution functions. The U-U pair distribution function for mixtures with a composition equal to or above a fractional $UCl_3$ concentration of 0.36 maintain the same shape and height as in pure $UCl_3$ (they essentially overlap), which emphasizes the importance of network formation in the mixtures. Below a fractional concentration of 0.36 the U-U pair distribution function rapidly deviates from the pure $UCl_3$, indicating an inability to maintain the favorable network structure. This behavior is visible in the third coordination shell in Figure 3.10. Related changes may be observed in other distribution functions. The location of this transition coincides with the minimum in the mixing energy and the maximum deviation of the density from an ideal solution (compare Figures 3.10, 3.6 and 3.9). In turn, these coincide with the eutectic composition according to the experimental phase diagram [29]. Combined with the evolution of the U-Cl and U-U pair distribution functions in the mixtures, this suggests that the negative mixing energy is driven by increases in the Cl coordination around U ions, but if the fractional $UCl_3$ concentration is below $\approx 0.36$, the gain from increasing this U-Cl coordination is countered by not being able to maintain the favorable U-U coordination seen in $UCl_3$, as evidenced by the break-up of the network structure. The

balance of the increase in the U-Cl coordination and decrease in U-U coordination as function of the composition of NaCl-$UCl_3$ salts is responsible for the minimum in the mixing energy and by extension the location of the eutectic point in the phase diagram.

The negative deviation from an ideal solution exhibited by the density implies that the volume increases. Often, a negative mixing energy is associated with a stronger bonding and lower volume, clearly that is opposite to what is observed for NaCl-$UCl_3$. The reason for increased volume and decreased density is again related to the evolution of the pair distribution function. The increased coordination number of Cl around U ions means that the bonding environment starts to resemble that of $U^{4+}$ ions in $UCl_4$, which may also be what drives the favorable interaction. The density of $UCl_4$ is noticeably lower (and the molar volume higher) than that of $UCl_3$, which we believe correlates with the negative deviation form an ideal mixture for the density of NaCl-$UCl_3$ mixtures. Note that this analogy does not imply presence of formal $U^4+$ ions in NaCl-$UCl_3$, but a partial transition that drives the evolution of both the mixing energy and density. Additional simulations and experiments would be required to prove this hypothesis.

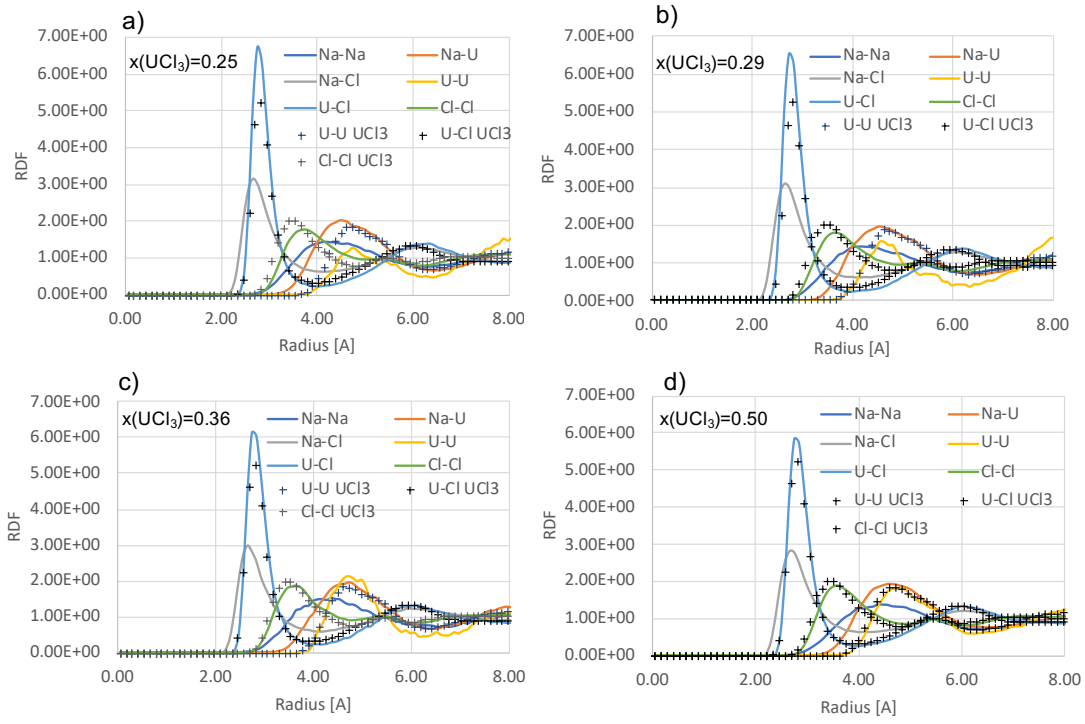


Figure 3.10: Pair distribution functions for NaCl-$UCl_3$ mixtures as function of composition ($x_{UCl_3} = 0.25$, $x_{UCl_3} = 0.29$, $x_{UCl_3} = 0.36$ and $x_{UCl_3} = 0.50$). The reference U-Cl and U-U pair distribution functions for $UCl_3$ are plotted in each figure for comparison.

# 4 Ab initio molecular dynamics simulations of select thermophysical and thermodynamic properties of the KCl-$UCl_3$ and $AlCl_3$-$UCl_3$ systems

The methodology applied to NaCl-$UCl_3$ in the previous chapter was directly translated to the KCl-$UCl_3$ and $AlCl_3$-$UCl_3$ systems. The KCl-$UCl_3$ system is very similar NaCl-$UCl_3$ due to the similarities between Na and K. However, as already discussed in the first chapter, $AlCl_3$ exhibits significantly different properties, which is evidenced by, for example, a much lower boiling point and a narrow temperature range where the molten phase is stable. The challenges associated with this salt and its mixtures will be further discussed below.

## 4.1 Review of experimental and modeling studies of KCl, KCl-$UCl_3$, $AlCl_3$ and $AlCl_3$-$UCl_3$

Density correlations for KCl and $AlCl_3$ have been reported by Janz et al. [18]. The KCl behavior is well-characterized, but the $AlCl_3$ density relation relies on only a small number of data points that are very close in temperature. The mixing energy between $UCl_3$ and KCl can be derived from the Calphad model due to Yin et al. [29], but to the best of our knowledge there is no direct experimental data. No data is available for $AlCl_3$ mixed with $UCl_3$. Modeling studies have been performed for some properties of the KCl system or mixtures including KCl [45, 46], but the ternaries that include uranium ions have received little attention.

## 4.2 Methodology

As already mentioned, the methodology for the KCl-$UCl_3$ and $AlCl_3$-$UCl_3$ systems is directly inherited from the NaCl-$UCl_3$ system. For K we used the PAW potential that includes the p electrons as valance states. For Al, the s and p electrons were treated as valance states. The optimized supercell sizes obtained for the NaCl-$UCl_3$ system were adopted for KCl-$UCl_3$ and $AlCl_3$-$UCl_3$. Both the D3 [2, 35] and dDsC [13, 38] methodologies were used to describe the dispersion interactions. So far, the mixed KCl-$UCl_3$ salts were only investigated at 1250 K. This range will be expanded in future work.

## 4.3 Results

### 4.3.1 Ab initio molecular dynamics simulations on KCl

#### Density

Figure 4.1a) plots the predicted density of molten KCl as function of temperature for the DFT-D3 and dDsC models. The correlation due to Janz et al. [18] derived from experimental data is also shown. The simulation results mimic the findings for NaCl, with the best agreement obtained for the dDsC dispersion model, which is within 5% or less of the experimental correlation across an extended temperature range. The calculated (dDsC) and experimental correlation for the density as function of temperature is listed in Table 4.1.

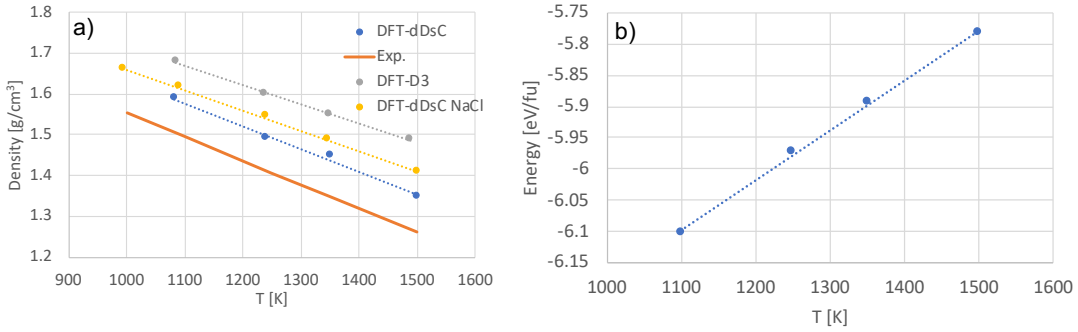


Figure 4.1: Density of KCl predicted with two different models for dispersion forces. Experimental data is represented by the correlation plotted as an orange line [18]. The lines shown are least-squares fits to the calculated data points. b) Calculated total energy of KCl as function of temperature. The line is a least-squares fit to data points and the slope represents the heat capacity.

| | Density (g/cm$^3$) | Heat capacity (J/mol/K) |
|---|---|---|
| KCl Calculated (dDsC) | $-0.000559T + 2.1921$ | 77.19 |
| KCl Experiment | $-0.000583T + 2.1357$ [18] | 73.60 [41] |
| $AlCl_3$ Calculated (dDsC) | $-0.00113T + 2.039$ | 76.28 |
| $AlCl_3$ Experiment | $-0.00271T + 2.565$ [18] | 125.5 [41] |

Table 4.1: Calculated and experimental correlations and values for density and heat capacity for KCl and $AlCl_3$.

#### Heat capacity

Figure 4.1b) plots the total energy per formula unit of molten KCl as function of temperature. The derivative equals the heat capacity of KCl, which is also tabulated in Table 4.1 together with an experimental reference value [41]. The simulation results indicate an approximately constant heat capacity, though in order to identify a small deviation from this linear relation a denser

temperature mesh would be required. The calculated heat capacity agrees very well with the experimental reference value [41].

### 4.3.2 Ab initio molecular dynamics simulations on $AlCl_3$

#### Density

The predicted density of molten $ACl_3$ is plotted in Figure 4.2a) from 450 K to 900 K, which also includes the correlation from Janz et al. [18]. The range of temperatures is chosen based on the experimental melting temperature of 453 K. The simulated data is off from experiments by a larger amount than seen for either NaCl, KCl or $UCl_3$. The deviation is not a constant shift, but rather the predicted temperature dependence is significantly off from the experimental data. As emphasized in the first chapter, the bonding in $AlCl_3$ is complex and it is feasible that the DFT methodology applied here is not capable of capturing all subtleties. However, it is also possible that the experimental data is inaccurate. The experimental correlation shown in Figure 4.2a) was derived from only two data points close to 450 K and only about 10 K apart. The resulting temperature dependence is steep and extrapolation suggest that density would go to zero at 950 K. Even though this is above the boiling point, we believe that the strong temperature dependence is odd and deserves further attention to confirm or refute.

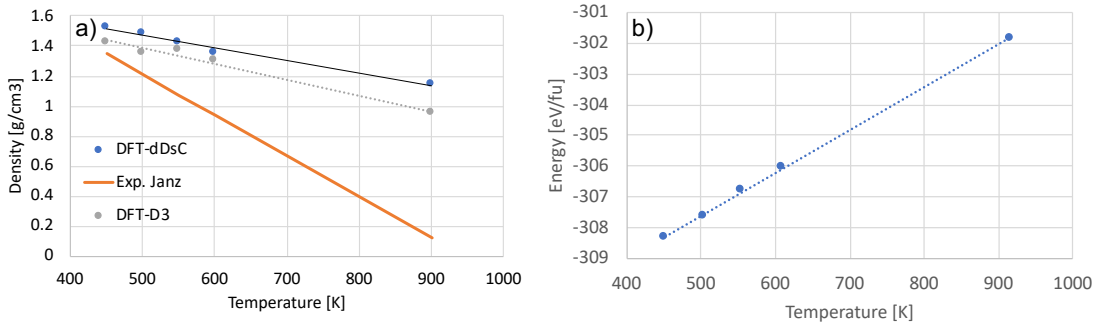


Figure 4.2: a) Density of $AlCl_3$ predicted with different models for the dispersion forces. Experimental data is represented by the correlation plotted as an orange line [18]. The lines are least-squares fits to the calculated data points, the equations of which are summarized in Table 4.1. b) Calculated total energy of $AlCl_3$ as function of temperature. The line is a least-squares fit to data points and the slope represents the heat capacity. Note that the point at 900 K is above the experimental boiling point, but still included in the simulations and seems to approximately follow the trend observed in the liquid range.

#### Heat capacity

Figure 4.2b) plots the total energy as function of temperature, from which the heat capacity can be derived by calculating the slope. The total energy closely follows a linear relation as function of temperature and, consequently, the heat capacity can be approximated as a constant in the temperature range investigated. The resulting heat capacity is listed in Table 4.1. Just as for the

density, there is a significant difference between the calculated and experimentally reported heat capacity [41]. Further investigations are needed to explain this discrepancy.

### 4.3.3 Ab initio molecular dynamics simulations on KCl-$UCl_3$

#### Density and structure

The densities of KCl-$UCl_3$ mixtures were calculated for the dDsC dispersion model at 1250 K and are shown in Figure 4.3a). The calculated densities are compared to experimental data from Janz et al. [18], Desyatnik et al. [47] as well as the previously calculated results for NaCl-$UCl_3$. Figure 4.3b) shows the corresponding deviation from ideal solution behavior. The challenge of converging the AIMD simulations leads to some scatter. We expect the scatter to decrease as better statistics are accumulated in ongoing simulations. Nevertheless, we conclude that the qualitative behavior is similar to the NaCl-$UCl_3$ system, but with about twice the deviation form ideal solution behavior. The maximum deviation from ideal solution behavior is again observed around a $UCl_3$ content of 0.35, which coincides with the eutectic composition for KCl-$UCl_3$ system. Unlike the NaCl-$UCl_3$ system, the KCl-$UCl_3$ system exhibits a negative deviation from an ideal solution across the full composition range. Recall that the NaCl-$UCl_3$ system had a positive or much closer to zero deviation in the $UCl_3$ rich range. The experimental data from Janz et al. [18] is in poor agreement with the calculated densities, both for absolute densities and the deviation from ideal solution behavior. However, the same quantities agree at least qualitatively with the densities reported by Desyatnik et al. [47]. Even though the latter predicts slightly higher deviation from ideal solution behavior, the shape of the concentration dependence is almost exactly reproduced. The discrepancy may be within the uncertainty of both experiments and simulations.

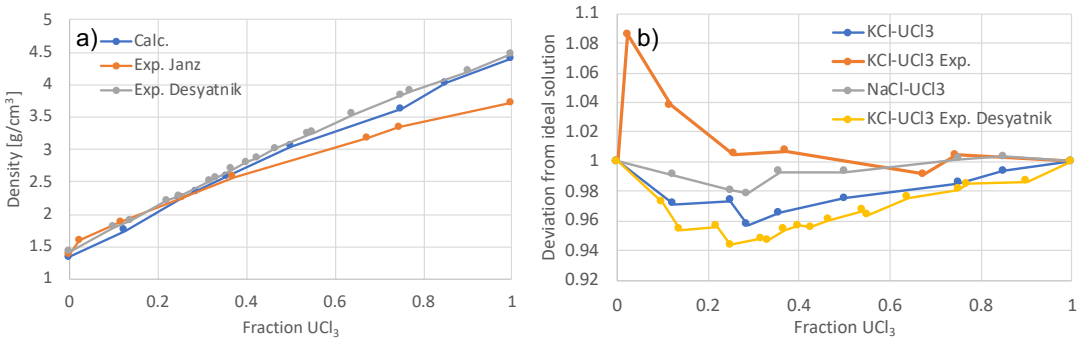


Figure 4.3: a) Density of KCl-$UCl_3$ mixtures obtained from simulations and experimental data [18,47] at 1250 K. b) Deviation of density from ideal solution behavior plotted as function of composition at 1250 K.

#### Mixing energy

The KCl-$UCl_3$ mixing energy at 1250 K is plotted in Figure 4.4, which also contains a correlation derived from a CALPHAD assessment of the KCl-$UCl_3$ system [29] and the AIMD prediction

for NaCl-$UCl_3$. The predicted mixing energy follows the CALPHAD assessment pretty closely, with slightly better agreement on the $UCl_3$ rich side. The minimum (most negative) mixing energy is about twice as large as for NaCl-$UCl_3$, but the shape of the mixing energy curve is similar for the two cases with a minimum close to a uranium content of 0.35, which again coincides with the eutectic composition. From this we conclude that the behavior of the mixing energy follows the same trend as for the density and also mimics the behavior of the NaCl-$UCl_3$ system. The correlation between density, mixing energy and the pair distribution function discussed for the NaCl-$UCl_3$ system also extends to KCl-$UCl_3$, however the detailed analysis is not included in this report since it is still ongoing.

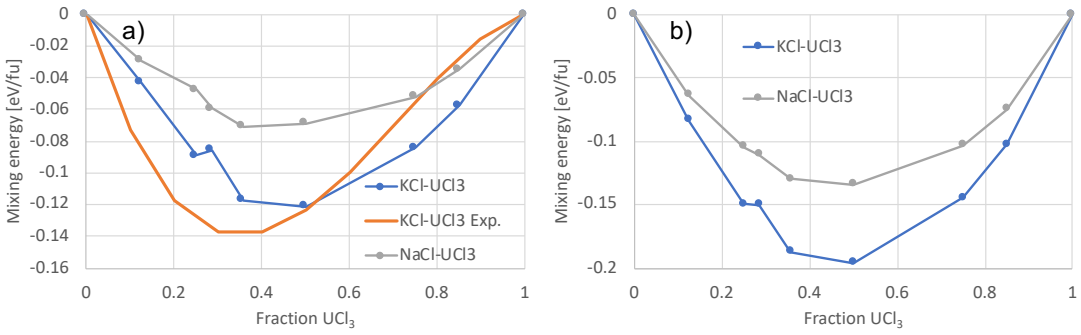


Figure 4.4: a) Mixing energies for KCl-$UCl_3$ at 1250 K. Pure KCl and $UCl_3$ are used as references. b) The KCl-$UCl_3$ free energy of mixing at 1250 K assuming an ideal solution.

### 4.3.4 Ab initio molecular dynamics simulations on $AlCl_3$-$UCl_3$

Simulations were also performed for $AlCl_3$-$UCl_3$ mixtures, however they are more challenging because of issues converging the electronic self-consistency cycles in VASP. Work is ongoing to resolve this issue. For this reason, it is premature to present any data. The problem is likely related to to the unique behavior $AlCl_3$ already discussed.

# 5 Summary and conclusions

Fundamental molten salt thermodynamic and thermophysical properties (e.g., density, heat capacity, viscosity, and thermal conductivity) are important for the development of next-generation molten salt reactors (MSRs), in which molten salts are used as both coolant and fuel. However, due to the corrosive nature of molten salts, measurements of their properties at high temperatures can be experimentally challenging. This is even more pertinent for fuel salts, which, in addition, contain toxic and radioactive actinides (U, Pu) as fuel and after burnup a range of fission products, all of which may influence properties. Using atomic scale simulations to fill these data gaps and to provide mechanistic understanding of property relations would facilitate more accurate evaluation of various concepts by reactor designers, developers and other interested parties. Modeling and simulations have an important role to play in reducing data gaps, because the compositional space of interest is extensive and difficult to cover with experiments alone, especially since some of the salts are also highly toxic or radioactive.

We have performed classical molecular dynamics (MD) and ab initio molecular dynamics (AIMD) simulations to predict the thermophysical properties of pure chloride salts and their mixtures in the $AlCl_3$-NaCl-KCl system over a wide temperature range from 800 K to 1400 K. Classical MD simulations are used for properties that require long simulation times, in particular thermal conductivity and viscosity. Our classical MD simulations used a non-polarizable Buckingham pair potential in combination with a Stillinger-Weber three-body potential for Al-Cl-Cl interaction, which were parameterized using ab initio calculated data such as equilibrium lattice parameters and single-crystal elastic constants. MD predicted thermophysical properties were compared with experimental data when they exist. In most cases, the agreement is good, which emphasizes the ability of the modeling and simulation approach to generate data for properties of molten salts with complex chemistry.

In addition, AIMD simulations relying on different models for Van der Waals interactions were used to predict temperature dependent thermophysical (density and thermal expansion) and thermodynamic (mixing energy and heat capacity) properties of NaCl, KCl and $AlCl_3$ mixed with $UCl_3$. The main topic of the present study is $UCl_3$ mixed with KCl and $AlCl_3$, however, the study of NaCl-$UCl_3$ performed in previous years under NEAMS and currently under another program (LANL LDRD) provided the theoretical basis for the KCl-$UCl_3$ and $AlCl_3$-$UCl_3$ studies. AIMD simulations of the pure end-member systems are able to accurately reproduce experimental data on densities and heat capacities provided that Van der Wals interactions are included in the simulations. The best agreement is obtained for the dDsC correlation. The simulations for $AlCl_3$ predict properties that deviate the most from experiments among the investigated systems, which could be related to the less ionic character of this system resulting in somewhat unique properties such as a very low boiling point. However, we speculate that there may also be substantial uncertainty in the experimental measurements.

Mixtures of $UCl_3$ with NaCl and KCl exhibit a negative mixing energy, with a minimum close

to the eutectic composition of $x_{UCl_3} = 0.35$. The magnitude of the minimum mixing energy is lower for KCl than for NaCl. For NaCl-$UCl_3$ the mixing energy is predicted to be independent of temperature. The corresponding mixing data as function of temperature has not yet been accumulated for KCl-$UCl_3$, but that system is expected to behave in the same way. The predicted mixing energy for NaCl-$UCl_3$ agree very well with available experimental data and for KCl-$UCl_3$ the predictions are consistent with an available CALPHAD assessment. The existence of a minimum for mixing energy is related to the evolution of the radial distribution function. Addition of NaCl to $UCl_3$ increases the U-Cl coordination, which is a favorable reaction. Up until $x_{UCl_3} = 0.35$ the system is able to increase this coordination number, while maintaining the intermediate range U-U correlation. This behavior is a consequence of the tendency of $UCl_3$ to form network structures. For a $UCl_3$ fraction less than approximately 0.35, the U-U coordination starts to decrease and deviate from pure $UCl_3$, which leads to a lower mixing energy (less favorable). The $x_{UCl_3} = 0.35$ composition coincides with the observed eutectic composition. The correlation between pair distribution functions and mixing energies extend to the KCl-$UCl_3$ system. The same interactions that control the mixing energy also govern the evolution of the density for mixed salts. Both KCl-$UCl_3$ and NaCl-$UCl_3$ exhibit a maximum deviation from ideal solution behavior at $x_{UCl_3} = 0.35$. The densities of the mixed salts are lower than for the ideal mixture. The maximum deviation is about 2% for NaCl-$UCl_3$ and 3% for KCl-$UCl_3$. The temperature dependence was only investigated for the NaCl-$UCl_3$ system, but KCl-$UCl_3$ is expected to behave in a similar way. The maximum deviation is only weakly dependent on temperature, but the deviation from ideal solution behavior exhibits some temperature dependence in the $UCl_3$ rich range. The predicted densities for the mixed systems agree at least qualitatively with available experimental data. New experiments would be required to assess the quantitive accuracy of the simulations.

The $AlCl_3$-$UCl_3$ is challenging to study with AIMD simulations, because of issues converging the electronic self-consistency cycles. We are currently working on resolving these issues. For this reason, no reliable data is yet available for this mixed system.

Future work will accumulate better statistics for the NaCl-KCl-$AlCl_3$-$UCl_3$ systems and their properties, extend simulations on KCl-$UCl_3$ to additional temperatures following the recipe presented for NaCl-$UCl_3$ and improve the methodology for $AlCl_3$-containing salts such that their unique properties can be captured and studied. On the potential development side, the impact of including polarization effects will be investigated. After completing these steps, the same methodology will be extended to other molten salt systems.

# Acknowledgements

This work was funded by the U.S. Department of Energy (DOE), Office of Nuclear Energy, Nuclear Energy Advanced Modeling and Simulation (NEAMS) program. Los Alamos National Laboratory, an affirmative action/equal opportunity employer, is operated by Triad National Security LLC, for the National Nuclear Security Administration of the U.S. Department of Energy under Contract No. 89233218CNA000001. Los Alamos Laboratory Directed Research and Development (LDRD) is acknowledged for supporting method development and establishing simulations procedures used in part of this study.

# References


[1] P. N. Haubenreich, J. R.Engel, Experience with the molten-salt reactor experiment, Nuc. Appl. Technol. 8 (1970) 118.

[2] B. Li, S. Dai, D.-E. Jiang, First-principles molecular dynamics simulations of $UCl_n$-NaCl (n = 3, 4) molten salts, ACS Appl. Energy Mater. 2 (2019) 2122.

[3] B. Li, S. Dai, D. en Jiang, Molecular dynamics simulations of structural and transport properties of molten NaCl-$UCl_3$ using the polarizable-ion model, J. Mo. Liq. 299 (2020) 112184.

[4] H. O. Nam, A. Bengtson, K. Vörtler, S. Saha, R. Sakidja, D. Morgan, First-principles molecular dynamics modeling of the molten fluoride salt with Cr solute, J. Nucl. Mater. 449 (2014) 148.

[5] H. O. Nam, D. Morgan, Redox condition in molten salts and solute behavior: A first-principles molecular dynamics study, J. Nucl. Mater. 465 (2015) 224.

[6] J. Song, S. Shi, X. Li, L. Yan, First-principles molecular dynamics modeling of $UCl_3$ in LiCl-KCl eutectic, J. Mol. Liq. 234 (2017) 279–286.

[7] R. A. Buckingham, The classical equation of state of gaseous helium, neon and argon, Proc. Royal Soc. London. Series A, Math. Phys. Sci. 168 (1938) 264 – 283.

[8] S. Grimme, Semiempirical GGA-type density functional constructed with a long-range dispersion correction, J. Comput. Chem. 27 (2006) 1787 – 1799.

[9] F. H. Stillinger, T. A. Weber, Computer simulation of local order in condensed phases of silicon, Phys. Rev. B 31 (1985) 5262 – 5271.

[10] K. Balasubrahmanyam, L. Nanls, Raman spectra of liquid $AlCl_3$-KCl and $AlCl_3$-NaCl, J. Chem. Phys. 42 (1965) 676 – 680.

[11] Y. S. Badyal, D. A. Allent, R. A. Howe, The structure of liquid $AlCl_3$ and structural modification in $AlCl_3$-MCl (M=Li, Na) molten salt mixtures, J. Phys.: Condens. Matter 6 (1994) 10193 – 10220.

[12] G. Kresse, J. Furthmuller, Efficient iterative schemes for ab initio total-energy calculations using a plane-wave basis set, Phys. Rev. B 54 (1996) 11169–11186.

[13] S. N. Steinmann, C. Corminboeuf, Comprehensive benchmarking of a density-dependent dispersion correction, J. Chem. Theory Comput. 7 (2011) 3567 – 3577.

[14] S. Plimpton, Fast parallel algorithms for short-range molecular dynamics, J. Comput. Phys. 117 (1995) 1 – 19.

[15] F. Muller-Plathe, A simple nonequilibrium molecular dynamics method for calculating the thermal conductivity, J. Chem. Phys. 106 (1997) 6082 – 6085.

[16] F. D. Murnaghan, The compressibility of media under extreme pressures, PNAS 30 (1944) 244 – 247.

[17] S. Takahashi, T. Muneta, N. Koura, H. Ohno, Structural analysis of the molten salt 50 mol% AlCl-50 mol% NaCl by x-ray diffraction, J. Chem. SOC.,Faraduy Trans. 2 81 (1985) 1107 – 1115.

[18] G. J. Janz, Thermodynamic and transport properties for molten salts: Correlation equations for critically evaluated density, surface tension, electrical conductance, and viscosity data, J. Phys. Chem. Ref. Data 17 (1988) 1 – 309.

[19] E. R. V. Artsdalen, I. S. Yaffe, Electrical conductance and density of molten salt systems: KCl-LiCl, KCl-NaCl and KCl-KI, J. Phys. Chem. 59 (1955) 118 – 127.

[20] R. W. Berg, H. A. Hjuler, B. N. J, Density of molten $NaAlCl_4$: A reinvestigation, J. Chem. Eng. Data 28 (1983) 251 – 253.

[21] H. A. Andreasen, N. J. Bjerrum, N. H. Hansen, Densities of molten $FeCl_3$, KCl-$FeCl_3$, and KCl-$AlCl_3$, J. Chem. Eng. Data 25 (1980) 236 – 239.

[22] T. Ejima, K. Shimakage, Y. Sato, H. Okuda, N. Kumada, A. Ishigaki, Viscosity measurement of alkali chlorides with capillary viscometer, NIPPON KAGAKU KAISHI 6 (1982) 961 – 968.

[23] B. Cleaver, P. Koronaios, Viscosity of the NaCl + $AlCl_3$ melt system, including the effect of added oxide, J. Chem. Eng. Data 39 (1994) 848 – 850.

[24] Y. Nagasaka, N. Nakazawa, A. Nagashima, Experimental determination of the thermal diffusivity of molten alkali halides by the forced rayleigh scattering method. i. molten LiCl, NaCl, KCl, RbCl, and CsCl, Int. J. Thermophys. 13 (1992) 555 – 574.

[25] N. Galamba, C. A. N. de Castro, J. F. Ely, Thermal conductivity of molten alkali halides from equilibrium molecular dynamics simulations, J. Appl. Phys. 120 (2004) 8676 – 8682.

[26] V. N. Desyatnik, S. F. Katyshev, S. P. Raspopin, Y. F. Chervinskii, Density, surface tension, and viscosity of uranium trichloride-sodium chloride melts, Sov. At. Energy 39 (1975) 649.

[27] H. Matsuura, R. Takagi, L. Rycerz, M. Gaune-Escard, Enthalpies of mixing in molten $UCl_3$-NaCl system, J. Nucl. Sci. Technol. 39 (sup3) (2002) 632–634.

[28] O. Benes, R. J. M. Konings, Thermodynamic evaluation of the NaCl-$MgCl_2$-$UCl_3$-$PuCl_3$ system, J. Nucl. Mater. 375 (2) (2008) 202–208.

[29] H. Yin, J. Lin, B. Hu, W. Liu, X. Guo, Q. Liu, Z. Tang, Thermodynamic description of the constitutive binaries of the NaCl-Cl-$UCl_3$-$PuCl_3$ system, Calphad 70 (2020) 101783.

[30] G. Kresse, D. Joubert, From ultrasoft pseudopotentials to the projector augmented-wave method, Phys. Rev. B 59 (1999) 1758–1775.

[31] P. E. Blöchl, Projector augmented-wave method, Phys. Rev. B 50 (1994) 17953–17979.

[32] A. I. Liechtenstein, V. I. Anisimov, J. Zaanen, Density-functional theory and strong interactions: Orbital ordering in mott-hubbard insulators, Phys. Rev. B 52 (1995) R5467–R5470.

[33] M. Cococcioni, S. de Gironcoli, Linear response approach to the calculation of the effective interaction parameters in the LDA + U method, Phys. Rev. B 71 (2005) 035105.

[34] S. L. Dudarev, D. N. Manh, A. P. Sutton, Effect of mott-hubbard correlations on the electronic structure and structural stability of uranium dioxide, Philos. Mag. B 75 (5) (1997) 613–628.

[35] S. Grimme, S. Ehrlich, L. Goerigk, Effect of the damping function in dispersion corrected density functional theory, J. Comp. Chem. 32 (7) (2011) 1456–1465.

[36] M. Dion, H. Rydberg, E. Schröder, D. C. Langreth, B. I. Lundqvist, Van der waals density functional for general geometries, Phys. Rev. Lett. 92 (2004) 246401.

[37] J. ří Klimeš, D. R. Bowler, A. Michaelides, Van der waals density functionals applied to solids, Phys. Rev. B 83 (2011) 195131.

[38] S. N. Steinmann, C. Corminboeuf, A generalized-gradient approximation exchange hole model for dispersion coefficients, The Journal of Chemical Physics 134 (4) (2011) 044117.

[39] H. Kim, J.-M. Choi, W. A. Goddard, Universal correction of density functional theory to include london dispersion (up to lr, element 103), J. Phys. Chem. Lett. 3 (3) (2012) 360–363.

[40] F. G. Edwards, J. E. Enderby, R. A. Howe, D. I. Page, The structure of molten sodium chloride, J. Phys., C, Solid State Phys. 8 (21) (1975) 3483–3490.

[41] Nist chemistry web book (2013).
URL `http://webbook.nist.gov/chemistry/`

[42] J. McMurray, private communication (2020).

[43] G. W. Neilson, A. K. Adya, S. Ansell, 8 neutron and x-ray diffraction studies on complex liquids, Annu. Rep. Prog. Chem., Sect. C: Phys. Chem. 98 (2002) 273–322.

[44] Y. Okamoto, F. Kobayashi, T. Ogawa, Structure and dynamic properties of molten uranium trichloride, J. Alloy. Compd. 29 (1998) 355–358.

[45] A. Bengtson, H. O. Nam, S. Saha, R. Sakidja, D. Morgan, First-principles molecular dynamics modeling of the LiCl-KCl molten salt system, Comput. Mater. Sci. 83 (2014) 362–370.

[46] C. Kwon, J. Kang, W. Kang, D. Kwak, B. Han, First principles study of the thermodynamic and kinetic properties of u in an electrorefining system using molybdenum cathode and LiCl-KCl eutectic molten salt, Electrochim. Acta 195 (2016) 216–222.

[47] V. N. Desyatnik, et al., Structure and dynamic properties of molten uranium trichloride, Zhurnl fizicheskoi khimii 50 (1976) 2522–2525.